Zeitschrift: Schweizerische mineralogische und petrographische Mitteilungen = Bulletin suisse de minéralogie et pétrographie

Band: 78 (1998)

Heft: 3

Artikel: Chemical characteristics of natural zirconolite

Autor: Gieré, Reto / Williams, C. Terry / Lumpkin, Gregory R.

DOI: https://doi.org/10.5169/seals-59299

SCHWEIZ. MINERAL. PETROGR. MITT. 78, 433–459, 1998

Chemical characteristics of natural zirconolite

by *Reto Gieré*[1], *C. Terry Williams*[2] and *Gregory R. Lumpkin*[3]

Abstract

Zirconolite ($CaZrTi_2O_7$) is a rare accessory mineral crystallizing under different geological conditions and in a wide range of generally SiO_2-poor rock types. In this paper, we present results obtained from a statistical study of nearly 300 chemical analyses of natural zirconolite. The chemical composition of natural zirconolite often deviates significantly from its theoretical composition due to extensive substitutions involving more than 30 chemical elements which vary widely in size (from 0.40 to 1.14 Å) and charge (from 2+ to 6+). These data document a high degree of compositional flexibility in zirconolite, and imply that availability of specific elements is a key factor in determining the chemical composition of zirconolite. The composition is strongly dependent on and reflects the chemical characteristics of the geological environment: zirconolite from lunar basalts is generally poor in Nb, Ta, U and Th, but rich in Fe, Zr, Hf and rare earth elements (ΣREE_2O_3 up to 32 wt%); zirconolite in metasomatically altered carbonate rocks exhibits a large variation in the content of U, Th and REE, but is generally low in Nb and Ta; and zirconolite from carbonatites is poor in Al and Mg, but extremely variable with respect to its Nb, Ta, REE, U and Th contents. Distinct compositional trends are observed for individual geological localities and are attributed to chemical variations resulting from pronounced continuous and discontinuous zoning within individual crystals.

The results show that the chemical composition of natural zirconolite can be simplified and satisfactorily described in terms of 9 components: Ca, Zr, Ti, Me^{5+} (Nb and Ta), Me^{3+} (mainly Al and Fe^{3+}), Me^{2+} (primarily Mg and Fe^{2+}), REE, ACT (U^{4+} and Th^{4+}), and O. In metasomatically altered carbonate rocks, most of the compositional variation can be expressed by the substitutions ACT + Me^{2+} ⇔ Ca + Ti and REE + Me^{3+} ⇔ Ca + Ti; the statistical analysis further indicates that both Fe^{2+} and Fe^{3+} are often present. In carbonatites, the most important substitution is Me^{5+} + Me^{3+} ⇔ 2 Ti , and Fe appears to be present predominantly as Fe^{3+}. The chemical data further suggest that Ca may be replaced by a limited amount of Mn^{2+} or Mg, and possibly by Zr.

Although many substitutions are theoretically possible, only a few are geologically important. The results suggest that the redox conditions during crystallization exert a significant control on the substitution mechanisms and possibly on the total amounts of ACT and REE accommodated by zirconolite. The highest reported amounts of ACT (0.475 ACT per formula unit), in particular, were incorporated by a substitution that requires the presence of a charge-balancing bivalent cation (ACT + Me^{2+} ⇔ Ca + Ti) and was thus influenced by the relative abundances of Fe^{2+} and Fe^{3+}. The limited number of important substitutions observed in natural samples indicates that these mechanisms produce zirconolite crystals with energetically favorable compositions and a generally high durability, implying that synthetic zirconolite designed for immobilization of high-level nuclear waste (e.g., in Synroc) should be tailored in a similar way.

Keywords: zirconolite, mineral chemistry, rare earth elements, actinides, substitution.

Introduction

Zirconolite, ideally $CaZrTi_2O_7$, is a relatively rare mineral reported to date from only 52 terrestrial localities, 7 lunar landing sites, and 1 meteorite (CABELLA and GAZZOTTI, 1994; DE HOOG and VAN BERGEN, 1996; PAN, 1997; RIED, 1994; SHENG et al., 1991; SONNENTHAL, 1992; WILLIAMS and GIERÉ, 1996). These occurrences, however, demonstrate that zirconolite can crystallize in a wide range of rock types and at different geological conditions. The mineral is easily overlooked

[1] Department of Earth and Atmospheric Sciences, Purdue University, West Lafayette, IN 47907-1397, USA. <giere@purdue.edu>
[2] Department of Mineralogy, The Natural History Museum, Cromwell Road, London SW7 5BD, U.K.
[3] Materials Division, Australian Nuclear Science and Technology Organisation, PMB 1, Menai 2234, NSW, Australia.

during microscopic examination of thin sections, because it may resemble more common accessory minerals such as ilmenite or rutile. Thus, the paucity of recorded occurrences may not accurately reflect the actual distribution of this mineral.

The chemical composition of natural zirconolite often deviates significantly from its theoretical composition due to extensive substitutions involving the rare earth elements (REE; including Y), the actinides (ACT), Nb, Fe and other elements. The available samples of naturally occurring zirconolite cover an extensive range in ACT content, age and host-rock type, and thus offer an ideal opportunity to study the relationships between α-decay doses, radiation damage, and geochemical alteration processes (see e.g., LUMPKIN et al., 1994a; LUMPKIN et al., 1998; LUMPKIN et al., 1994b; LUMPKIN et al., 1997). It is the purpose of the present paper to document and discuss the observed compositional variation of zirconolite in various geological environments. Moreover, we propose a series of substitutions and end-members which appear to be best suited to describe the natural chemical variation. Understanding the crystal chemistry of naturally occurring zirconolite is essential for the formulation of zirconolite-based crystalline wasteforms (e.g., Synroc) designed to immobilize high-level nuclear waste or excess weapons plutonium. Besides being an excellent natural analogue for such waste forms, the mineral is of considerable petrologic interest because its presence is controlled to a great extent by the bulk composition of the host rock and the fluid phase (ALLEN and ELLIS, 1996), and because its chemical zoning patterns may be useful indicators for changes that took place in the geological environment during crystallization and alteration (GIERÉ and WILLIAMS, 1992).

Crystal structure of zirconolite

The crystal structure of monoclinic zirconolite is closely related to those of fluorite and pyrochlore: it can be regarded, for instance, as an anion-deficient superstructure based on the fluorite struc-

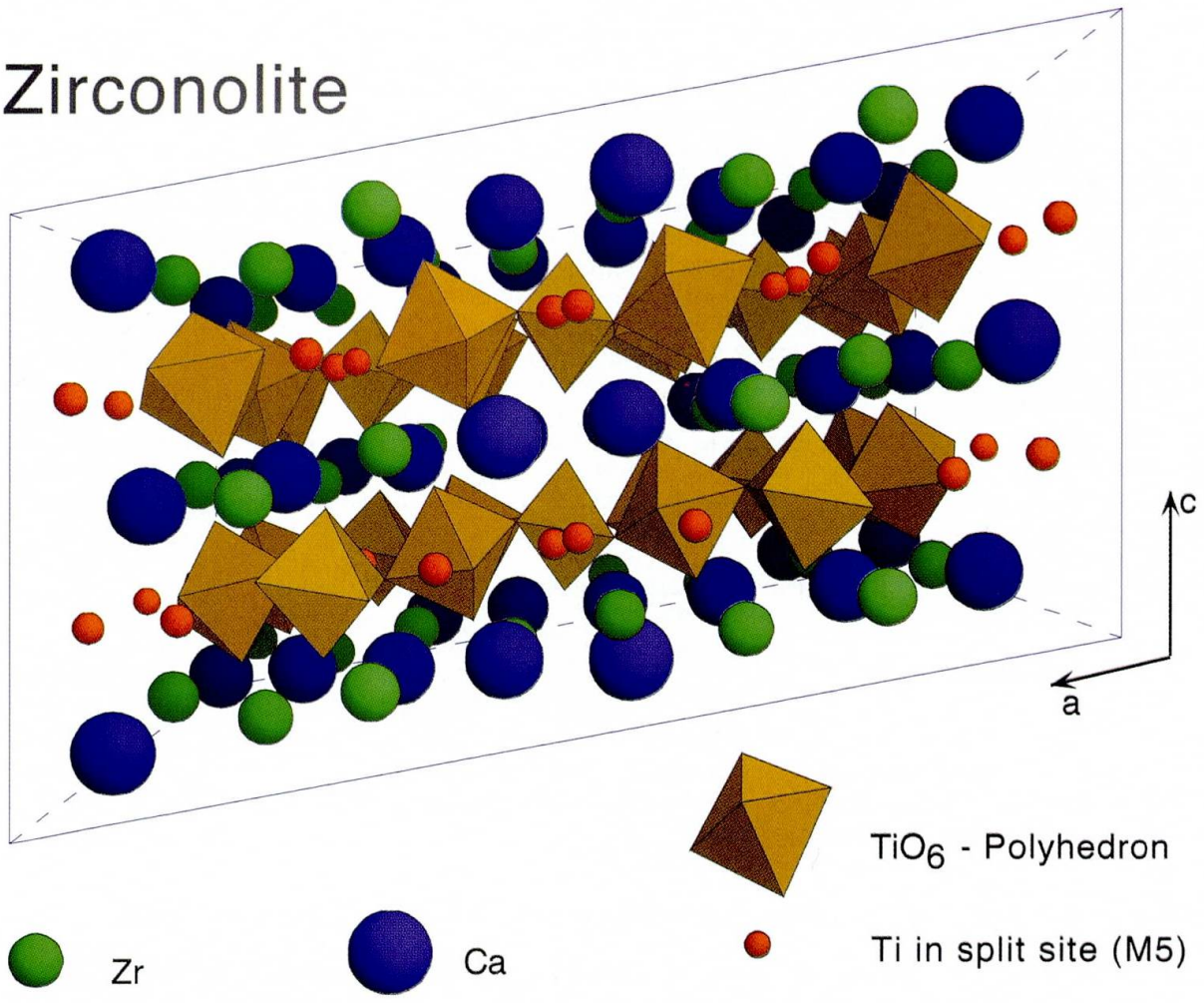

Fig. 1 Crystal structure of zirconolite-*2M*, drawn using data from GATEHOUSE et al. (1981).

ture (PYATENKO and PUDOVKINA, 1964). On the other hand, zirconolite can also be thought of as a derivative of the cubic pyrochlore structure ($A_2B_2X_6Y$, where cations are represented by A and B, anions by X and Y), in which three different cations (Ca, Zr, Ti) have ordered onto five different sites. A major difference between these two structures is that the B-X octahedra in pyrochlore are arranged in a three-dimensional array, whereas in zirconolite the Ti–O octahedra are arranged only in a two-dimensional array. Thus, the crystal structure of zirconolite is best described as a layer structure in which layers of Ti polyhedra lie parallel to (001) and alternate with planes containing Ca and Zr (Fig. 1). The Ti layer is built as a continuous sheet of six-membered corner-sharing TiO_6 rings (M6 sites) each of which surrounds a pair of statistically occupied sites containing Ti atoms coordinated by five oxygens in a trigonal bipyramid (split M5 site; shown as Ti atoms in Fig. 1). The Ca and Zr atoms (shown as spheres in Fig. 1) are arranged within the layers as alternating chains of distorted CaO_8 cubes (M8 sites) and ZrO_7 polyhedra (M7 sites; GATEHOUSE et al., 1981; ROSSELL, 1980; SINCLAIR and EGGLETON, 1982; SMITH and LUMPKIN, 1993; WHITE, 1984). The cation sites in the zirconolite structure have very different polyhedral volumes, ranging from 5.7 Å^3 for the M5 site to 21.3 Å^3 for the M8 site (FIELDING and WHITE, 1987), creating a structure capable of accommodating a wide variety of chemical elements.

Three polytypes of zirconolite have been reported in natural samples: zirconolite-*2M*, the two-layered monoclinic aristotype of the zirconolite minerals (WHITE et al., 1984); zirconolite-*3T*, a three-layered trigonal polytype, and zirconolite-*3O*, a three-layered orthorhombic polytype (BAYLISS et al., 1989; MAZZI and MUNNO, 1983). Two additional polytypes have recently been observed by high resolution transmission electron microscopy of synthetic samples; these polytypes, zirconolite-*4M* and zirconolite-*6T*, appear to be supercells of the zirconolite-*2M* and -*3T* structures, respectively (COELHO et al., 1997; SMITH and LUMPKIN, 1993). At the present state of knowledge, it is not possible to identify either the compositional field or the pressure and temperature conditions under which a specific polytype is stabilized relative to the others.

Chemical composition

A compilation of chemical analyses for natural zirconolite has been published recently (WILLIAMS and GIERÉ, 1996). This set of 321 analyses (an updated version is available from the authors) contains mainly data obtained by electron probe microanalysis (EPMA) but also some early wet chemical analyses of mineral separates. The latter, however, most likely do not fully characterise the chemical composition, because zirconolite often exhibits pronounced zoning and is invariably finely intergrown with other minerals. In the following discussion, we therefore only use the EPMA data (n = 291), supplemented in certain cases by analyses obtained through analytical transmission electron microscopy (AEM; for analytical method, see LUMPKIN et al., 1994c)

The review of WILLIAMS and GIERÉ (1996) has shown that both the range of elements accommodated in natural zirconolite and the degree of substitution are extensive. Thirty or more chemical elements are often present at the 0.1 to 1.0 wt% concentration level, and any microprobe analysis of natural zirconolite should include data for at least the following elements: Mg, Al, Si, Ca, Ti, Mn, Fe, Zr, Nb, Hf, Ta, W, Pb, Th, U, and of the REE group Y, La, Ce, Pr, Nd, and Gd. Some zirconolites may additionally contain Cr (particularly in lunar basalts) or Zn (in some metasomatic samples). Sr and Ba are only rarely detected (DE HOOG and VAN BERGEN, 1997; G.R. LUMPKIN, unpublished data). Pb is present in some cases only (up to 1.5 wt% PbO); its concentration is correlated with those of Th and U and with the age of the sample, and calculations have shown that most of the Pb is radiogenic (LUMPKIN et al., 1994b; and unpublished data). Na and K, although reported in some wet chemical analyses, have not been detected by EPMA, except in two samples, where zirconolite apparently contains small amounts of these elements (DE HOOG and VAN BERGEN, 1997; PAN, 1997). It is of note that low contents of Si (SiO_2 < 1 wt%) are common, and in some cases Si may be present at substantially higher concentrations, particularly in altered parts of zirconolite (LUMPKIN et al., 1994b; WILLIAMS et al., in prep.). There is some indication for the presence of H_2O in a number of samples due to their low oxide totals (PLATT et al., 1987; ZAKRZEWSKI et al., 1992), but zirconolite is, in general, anhydrous.

Some of the elements that are commonly below detection limit or present only at very low concentrations in natural zirconolite, may be introduced in substantial concentrations in synthetic crystals: in special Synroc formulations, for example, Na_2O and SrO can be incorporated at levels up to 2.4 wt% and 1.4 wt%, respectively (KESSON et al., 1983; LUMPKIN et al., 1991; LUMPKIN et al., 1995; RYERSON, 1984).

Zirconolite with an ideal $CaZrTi_2O_7$ stoichiometry theoretically contains 16.5 wt% CaO,

Tab. 1 Extent of site substitution in natural zirconolite.

Site	Element	Max./Min. % cation in site	Analysis number [1]	Host rock	Locality
M8	Σ(REE) [2]	78.8 (max.)	L11	Lunar Basalt	Apollo 15 Landing Site
	Σ(U + Th)	40.4 (max.)	M59	Metasomatic (vein)	Adamello, Italy
	Ca	21.2 (min.)	L11	Lunar Basalt	Apollo 15 Landing Site
M7	Hf	2.4 (max.)	L9	Lunar Basalt	Apollo 15 Landing Site
	Zr	97.6 (min.)	L9	Lunar Basalt	Apollo 15 Landing Site
M5,6	Mg	14.8 (max.)	NS14	Nepheline Syenite	Tchivira Mt., Angola
	Fe_{total}	30.5 (max.) [3]	L7	Lunar Lithic Fragment	Apollo 14 Landing Site
	Al	11.3 (max.) [4]	NS14	Nepheline Syenite	Tchivira Mt., Angola
	Σ(Nb + Ta)	41.2 (max.)	C15	Carbonatite	Kovdor, Russia
	W	1.1 (max.)	M8	Metasomatic (skarn)	Bergell, Switzerland/Italy
	Ti	34.8 (min.)	C71	Carbonatite	Kaiserstuhl, Germany

[1] Analysis numbers refer to table 3 in WILLIAMS and GIERÉ (1996)
[2] The abbreviation REE includes the lanthanides (La – Lu) as well as Y
[3] This value corresponds to 12.67 wt% Fe_2O_3, which is still higher than that recently reported for zirconolite from lavas in Eastern Indonesia (DE HOOG and VAN BERGEN, 1996)
[4] The highest recorded value of 13.5% (analysis C16) is suspect, because it is a wet chemical analysis on separated grains and is inconsistent with recent microprobe data

36.3 wt% ZrO_2, and 47.2 wt% TiO_2. In natural samples, CaO ranges from 2.63 to 16.5 wt%, ZrO_2 from 24.3 to 45.4 wt%, and TiO_2 from 13.6 to 45.9 wt%, showing that the major components can be substituted to a large extent by other elements. The variation in ZrO_2, however, is so large only on a wt% basis because it is mainly the result of extensive substitutions taking place on the Ca and Ti sites: nearly 80% of the M8 site and up to 65% of the M5,6 sites may be occupied by elements other than Ca and Ti, respectively, whereas at least 97% of the M7 sites are filled by Zr in all cases (Tab. 1). These relationships are shown graphically in figure 2, where most data points plot on the Zr-rich side of the theoretical zirconolite composition.

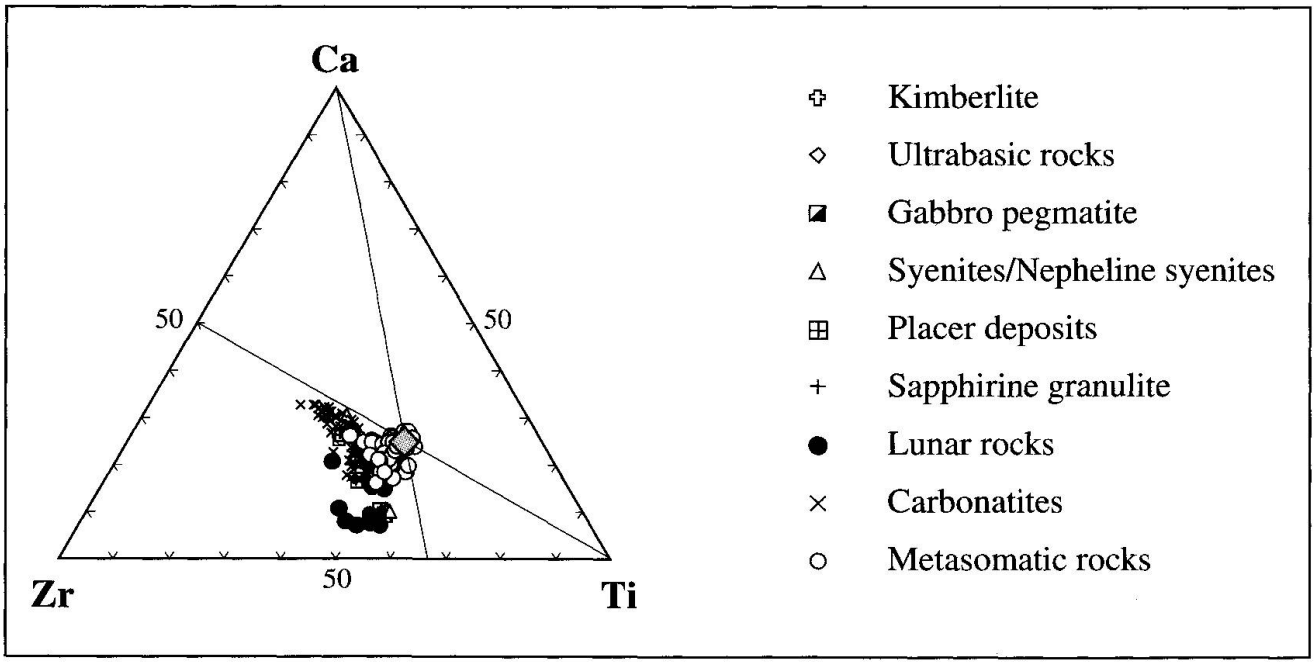

Fig. 2 Triangular diagram showing the compositional variation of natural zirconolite with respect to the major components Ca, Zr, and Ti (in atomic %). Shaded diamond represents the theoretical composition of pure $CaZrTi_2O_7$. Only EPMA data are plotted (n = 291; data from WILLIAMS and GIERÉ, 1996); AEM data not included.

Tab. 2 Selected hypothetical zirconolite end-members.

	M8	M7	M5,6	M5,6		Evidence [1]	
						natural [2]	synthetic [3]
1	Ca	Zr	Ti	Ti	O_7	x	x
2	Ca	Zr	Zr	Ti	O_7	*	x
3	Ca	Zr	Me^{5+}	Me^{3+}	O_7	x	x
4	Ca	Zr	W^{6+}	Me^{2+}	O_7	x	x
5	Ca	Ti	Ti	Ti	O_7		x
6	Ca	Hf	Ti	Ti	O_7	x	x
7	Ca	ACT	Ti	Ti	O_7	x	x
8	Ca	REE	Ti	Me^{5+}	O_7	x	x
9	ACT	Zr	Ti	Me^{2+}	O_7	x	x
10	ACT	Zr	Me^{3+}	Me^{3+}	O_7		x
11	REE	Zr	Ti	Me^{3+}	O_7	x	x
12	REE	Zr	Me^{5+}	Me^{2+}	O_7	x	x
13	REE	REE	Ti	Ti	O_7	*	x

[1] Except for end-members (1) and (3), none of the end-members occurs in nature nor has it been synthesized, but there is evidence for substitutions towards them

[2] * indicates that evidence is presented in this study

[3] E.R. VANCE, personal communication. Evidence for end-members (2) and (5) from GATEHOUSE et al. (1981)

The limited extent of Zr substitution in natural samples is in marked contrast to synthetic zirconolite: here, Zr may be replaced up to approximately 50% by ACT (e.g., U^{4+}, Pu^{4+}), 97% by Hf, and 50% by REE (e.g., Nd^{3+} or Ce^{4+}); the higher concentrations of ACT and REE tend to produce twinning and stacking disorders, and to develop the 4M polytype rather than the 2M polytype (BEGG and VANCE, 1997; BUCK and GIERÉ, in press; COELHO et al., 1997; E.R. VANCE, private communication; VANCE et al., 1995). Moreover, GATEHOUSE et al. (1981) reported that Zr can also be replaced by Ti; their synthetic zirconolite, in fact, conformed to the general formula $CaZr_xTi_{3-x}O_7$ ($0.85 \leq x \leq 1.30$). The latter takes into account that significant amounts Zr were also observed on the M5,6 sites (see also CHEARY and COELHO, 1997). GATEHOUSE et al. (1981) further showed that some Zr may be allocated on the M8 site. Limited evidence for some of these substitution mechanisms is also found in natural samples (see below).

In combination with the crystal structure refinements of GATEHOUSE et al. (1981) and SINCLAIR and EGGLETON (1982), the data for natural zirconolite document that the structure of zirconolite is compositionally very flexible on all sites. This indicates that availability of specific components must be a key factor in controlling the chemical composition of zirconolite. The chemical components incorporated into the zirconolite structure vary in size from 0.40 Å ($^{[6]}Si^{4+}$) to 0.83 Å (Mn^{2+}) on the M5,6 sites, from ~ 0.67 Å (Ti^{4+}) to ~ 1.04 Å (Nd^{3+}) on the M7 site, and from 0.84 Å (Zr^{4+}) to 1.26 Å (Sr^{2+}) on the M8 site (effective ionic radii from SHANNON, 1976). In general, the Ca site does not easily accommodate cations larger than Ce^{3+} (r = 1.143 Å for CN = 8; La commonly present only in small concentrations). This is due to the smaller volume of the Ca site in zirconolite relative to that in pyrochlore (SMITH and LUMPKIN, 1993). In natural samples, the most important substituents are: ACT and REE for Ca on the M8 site; Nb, Ta, Fe, Mg, and Al for Ti on the M5,6 sites; and Hf for Zr on the M7 site.

Because the zirconolite system comprises more than 30 components, it needs to be simplified in order to assess the crystal chemistry in terms of substitutions or exchange vectors. A first step in reducing the number of components is to ignore the radiogenic Pb. We further neglect the generally small quantities of Si which is most likely incorporated into zirconolite via a simple single-site substitution, i.e. $Si^{4+} \Leftrightarrow Ti^{4+}$; ignoring Si, therefore, does not directly affect other substitutions. A next step is to group bivalent, trivalent and pentavalent metal ions by defining the new variables

$$Me^{2+} = Mg^{2+} + Fe^{2+} + Mn^{2+} + Zn^{2+}$$
$$Me^{3+} = Al^{3+} + Fe^{3+} + Cr^{3+}$$
$$Me^{5+} = Nb^{5+} + Ta^{5+} .$$

With this measure, we ignore simple single-site substitutions such as e.g., $Mg^{2+} \Leftrightarrow Fe^{2+}$ and $Al^{3+} \Leftrightarrow Fe^{3+}$. We further constitute that only trivalent lanthanides (Ln) and Y^{3+} are included in the abbreviation "REE", given by:

$$REE = Ln^{3+} + Y^{3+} .$$

This term, therefore, does not account for Ln^{4+} which may be present in the Ca and Zr sites of synthetic zirconolite (e.g., Ce^{4+}; see BEGG et al.,

Tab. 3 Potentially important substitutions in zirconolite.

Substitution				Sites involved
1	Zr	⇔	Ti	M5,6
2	$Me^{5+} + Me^{3+}$	⇔	2 Ti	M5,6
3	$W^{6+} + Me^{2+}$	⇔	2 Ti	M5,6
4	$2\ Me^{3+}$	⇔	$Ti + Me^{2+}$	M5,6
5	$Me^{5+} + Me^{2+}$	⇔	$Ti + Me^{3+}$	M5,6
6	Ti	⇔	Zr	M7
7	Hf	⇔	Zr	M7
8	ACT	⇔	Zr	M7
9	$REE + Me^{5+}$	⇔	Zr + Ti	M5,6/M7
10	REE + Ti	⇔	$Zr + Me^{3+}$	M5,6/M7
11	REE + 2 Ti	⇔	$Zr + Me^{5+} + Me^{2+}$	M5,6/M7
12	$ACT + Me^{2+}$	⇔	Ca + Ti	M5,6/M8
13	$ACT + 2\ Me^{3+}$	⇔	Ca + 2 Ti	M5,6/M8
14	$ACT + Me^{3+}$	⇔	$Ca + Me^{5+}$	M5,6/M8
15	$ACT + Me^{3+}$	⇔	REE + Ti	M5,6/M8
16	$ACT + Me^{2+}$	⇔	$REE + Me^{3+}$	M5,6/M8
17	ACT + Ti	⇔	$REE + Me^{5+}$	M5,6/M8
18	$ACT + Ti + Me^{2+}$	⇔	$Ca + Me^{5+} + Me^{3+}$	M5,6/M8
19	$ACT + 2\ Me^{3+}$	⇔	$REE + Me^{5+} + Me^{2+}$	M5,6/M8
20	$REE + Me^{3+}$	⇔	Ca + Ti	M5,6/M8
21	$REE + Me^{5+} + Me^{2+}$	⇔	Ca + 2 Ti	M5,6/M8
22	REE + Ti	⇔	$Ca + Me^{5+}$	M5,6/M8
23	$REE + Me^{2+}$	⇔	$Ca + Me^{3+}$	M5,6/M8
24	$^{M8}REE + {}^{M7}REE$	⇔	Ca + Zr	M7/M8

1998). The last step consists in combining the most common tetravalent actinides in the abbreviation ACT, defined as:

$ACT = U^{4+} + Th^{4+}$.

This definition may be expanded to include other tetravalent actinides so as to account for, e.g., Np^{4+} and Pu^{4+} in studies on zirconolite-based nuclear waste forms. The trivalent transuranic actinides, although common constituents of high-level radioactive waste (e.g, Np^{3+}, Am^{3+}), should be grouped under REE, because they are incorporated into synthetic zirconolite in a way similar to that of REE (e.g., Nd^{3+}; VANCE et al., 1994). Hence, the number of components has been reduced to 11 (Ca, Zr, Ti, ACT, REE, Me^{2+}, Me^{3+}, Me^{5+}, W, Hf, O); these are used here to define 13 hypothetical end-members for the zirconolite system (Tab. 2). These end-members were chosen, because there is evidence from either natural or synthetic zirconolite for the existence of solid solution among them. It should be noted that end-member (13) represents a pyrochlore rather than zirconolite. Apart from stoichiometric $CaZrTi_2O_7$ and $CaZrMe^{5+}Me^{3+}O_7$, however, none of the other 10 zirconolite end-members has been found in nature nor have they been synthesized. Nonetheless, these hypothetical end-members are useful for defining substitutions (or exchange vectors) effective in the multicomponent zirconolite system. The potentially most important substitutions in zirconolite are listed in table 3 which, however, does not account for any of the possible single-site substitutions amongst Me^{2+}, Me^{3+} and Me^{5+} (see above). Several of the more complicated substitutions are linear combinations of simpler substitutions and were listed because they may be more suitable to describe compositional variations (see below).

In natural zirconolite, the extent of Zr substitution is limited (cf. Fig. 2, Tab. 1) and therefore, in a first approach, the Zr-free end-members (5), (6), (7), (8), and (13) can be disregarded when studying natural zirconolite. End-member (4) is of minor importance, because W was detected in a few samples only and generally in small concentrations (Tab. 1). Moreover, evidence for substitution towards end-members (2) and (10) has so far only been found in synthetic zirconolite. These observations suggest that the chemical composition of natural zirconolite can be satisfactorily described in terms of the 5 end-members $CaZrTi_2O_7$, $CaZrMe^{5+}Me^{3+}O_7$, $ACTZrTiMe^{2+}O_7$, $REEZrTiMe^{3+}O_7$, and $REEZrMe^{5+}Me^{2+}O_7$. The latter and the respective exchange vectors, thus, define the composition space of natural zirconolite which may be graphically represented as a double tetrahedron (Fig. 3). One of the advantages of choosing this representation is that the composition space can be subdivided into a Me^{2+}- and a Me^{3+}-dominated portion located in the lower left and

upper right part of the double tetrahedron, respectively. Below, we will use this composition space and parts thereof to describe the chemical variation observed in zirconolite from different geological environments.

Petrographic features of zirconolite and its host rocks

Zirconolite has been described from a variety of host rocks including kimberlite, ultrabasic rocks, dendritic anorthosite, gabbro pegmatite, syenite, nepheline syenite, carbonatite, metasomatic and metamorphic rocks (including rodingites; A. STUCKI, personal communication), as well as placer deposits (Tab. 4). In lunar samples, zirconolite was found primarily in coarse-grained basalts, but was also reported from feldspathic peridotite, lithic fragments, and metamorphosed breccia. In meteorite samples, zirconolite has so far been observed only from plagioclase-olivine inclusions in the Allende carbonaceous chondrite (SHENG et al., 1991). A common feature of all these host rocks is their low SiO_2 content and, in most cases, the absence of quartz. To our knowledge, quartz as a rock-forming mineral has only been described from two zirconolite-bearing samples, a dendritic anorthosite from the Skaergaard intrusion, East Greenland (SONNENTHAL, 1992) and a gabbro pegmatite on St. Kilda, Scotland (HARDING et al., 1982). So far, only one locality is known where zirconolite occurs in relatively evolved rocks (K-rich lavas with 57–62 wt% SiO_2), in which it is associated with a hydrated silica phase (DE HOOG and VAN BERGEN, 1996). To date, carbonatite, with sixteen reported occurrences of zirconolite, is the most common host rock for this mineral (WILLIAMS and GIERÉ, 1996). In all these rock types, zirconolite occurs as an accessory mineral. It is usually less than 100 μm in size, but cm-sized crystals have been found in heavy mineral sands of Sri Lanka and in the phoscorites at Phalaborwa, South Africa.

Because zirconolite exhibits a wide variation in composition, its optical properties as seen in thin section vary considerably. LAVEROV et al. (1996) recently reported optical properties for synthetic zirconolite, which formed as elongate prismatic crystals (up to 1 mm in length) upon cooling of a melt in the system $CaO–TiO_2–ZrO_2$; according to their observations, pure zirconolite

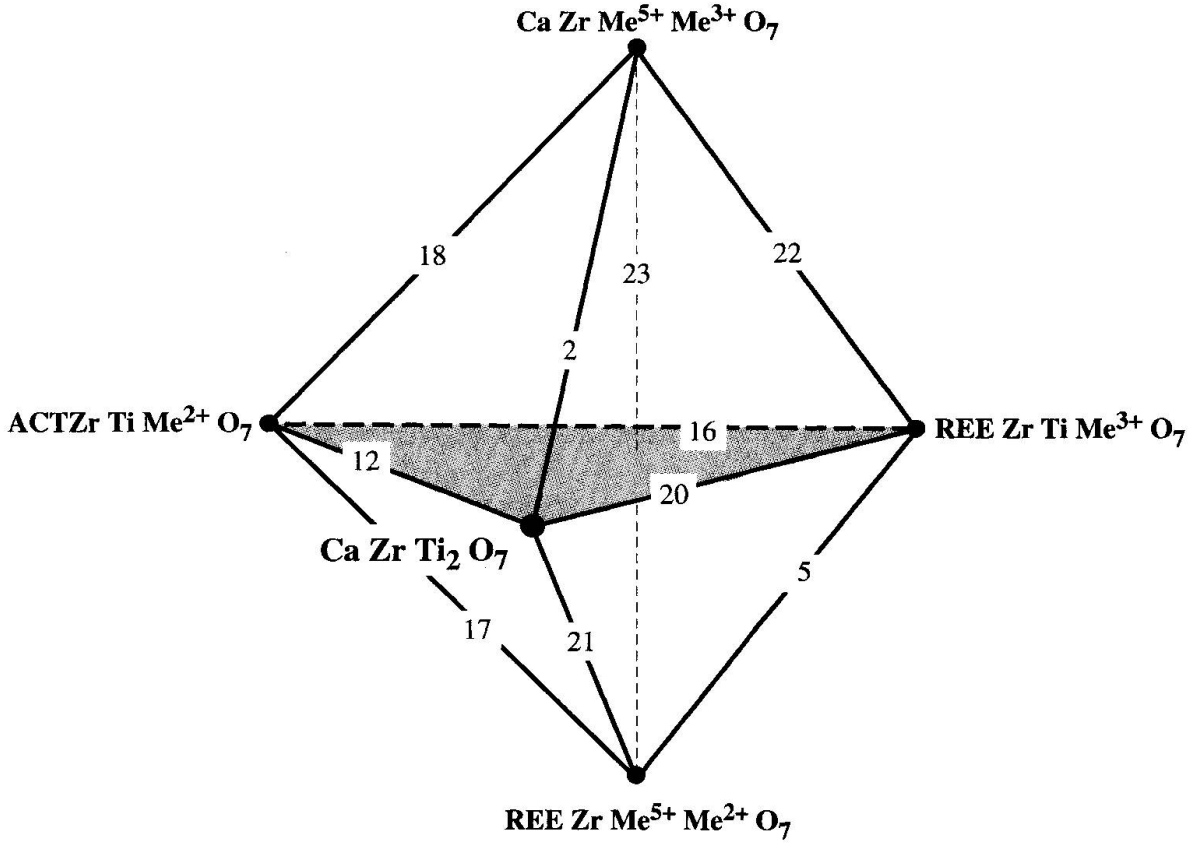

Fig. 3 Composition space for natural zirconolite. Note that upper right part of the double tetrahedron is Me^{3+}-dominated, whereas lower left is Me^{2+}-dominated. Numbers on tielines refer to substitutions listed in table 3. Shaded plane represents ternary system shown in figure 15b.

Tab. 4 Zirconolite and associated minerals in various host rocks. Minerals listed are either in grain contact or intergrown with zirconolite (most commonly observed minerals in capitals).

Rock type	Number of occurrences	Number of analyses [1]	Associated minerals
Kimberlite	3	1	Baddeleyite, calcite, ilmenite, zircon
Ultrabasic rocks [2]	3	3	Apatite, baddeleyite, zircon
Dendritic anorthosite	1	2 [3]	Allanite, apatite, baddeleyite, ilmenite, plagioclase, titanite, zircon
Gabbro pegmatite	1	1	Allanite, apatite, biotite, epidote, titanite, zircon
Syenite	5	4	Allanite, APATITE, epidote, ILMENITE, titanite, zircon
Nepheline syenite	6	21	Apatite, BADDELEYITE, hellandite, hibonite, perovskite, pseudobrookite, wöhlerite, zircon
Calc-alkaline lava	1	0 [4]	Hydrated silica
Carbonatite	16	142	Anatase, APATITE, BADDELEYITE, CALZIRTITE, clinohumite, magnetite, perovskite, PYROCHLORE, wöhlerite, zircon
Metasomatically altered rocks	11	98	Allanite, APATITE, baddeleyite, betafite, CALCITE,chlorite, diopside, dissakisite-(Ce), DOLOMITE, GEIKIELITE, ilmenite, jordisite, olivine, PHLOGOPITE, pyrite, pyrrhotite, rosenbuschite, rutile, SPINEL, titanite, titanian clinohumite, zircon
Sapphirine granulite	1	3	Enstatite, phlogopite, sapphirine, spinel
Cordierite gneiss	1	2 [5]	Rutile, titanite, zircon
Alnöite	1	0	Baddeleyite, perovskite
Placer	2	5	Baddeleyite and perovskite from heavy mineral fraction
Lunar rocks	7	13	BADDELEYITE, ilmenite
Meteorite [6]	1	0	Perovskite, olivine, plagioclase

[1] Electron microprobe analyses used for this paper; data listed by WILLIAMS and GIERÉ (1996)
[2] Includes zirconolite in chromitite layers (no analyses given by CABELLA and GAZZOTTI, 1994)
[3] Analyses given by SONNENTHAL (1992)
[4] No analyses given by DE HOOG and VAN BERGEN (1996)
[5] Analyses listed by PAN (1997)
[6] No full analysis available (cf. SHENG et al., 1991)

of $CaZrTi_2O_7$ composition is colorless and biaxial negative, exhibits a high birefringence, and has straight extinction and negative elongation (2V = 80–85°, $n\gamma = 2.30$, $n\beta = 2.27$, $n\alpha = 2.23$, $n\gamma - n\alpha = 0.07$). Natural zirconolite may be translucent or opaque, and its color can vary from orange-red to reddish-brown or dark brown, and in many cases, several of its optical properties resemble those of rutile. If zirconolite is enriched in ACT, however, and when enclosed by phlogopite, it is usually surrounded by strongly pleochroic haloes (GIERÉ, 1990), a radiation damage feature not observed around rutile. D'OREY (1991) observed considerable anisotropy of microhardness values (ranging from 5.4 to 6.2 on the Mohs scale) for a Nb-rich zirconolite from Santiago island, Cape Verde.

In several localities, zirconolite represents the only Zr phase. More often, however, it is associated or intergrown with other Zr minerals, most commonly with baddeleyite (ZrO_2), calzirtite ($Ca_2Zr_5Ti_2O_{16}$), and zircon, but occasionally also with eudialyte, rosenbuschite or wöhlerite. A summary of the minerals found in close textural association with zirconolite is given in table 4. More detailed paragenetic information as well as a list of references may be found in the review of WILLIAMS and GIERÉ (1996).

Figure 4 shows the chemographic relationships for the ternary system $CaO–ZrO_2–TiO_2$. The diagram represents a projection from CO_2 and thus, can be used only if excess CO_2 is present (e.g., for carbonatites and metacarbonate rocks). Some of the minerals shown in figure 4 lie on pseudobinary joins, revealing two compositional degeneracies, i.e. baddeleyite – perovskite and calcite – rutile. This implies, for example, that calzirtite cannot coexist in equilibrium with both baddeleyite and perovskite in this simplified system. If zirconolite is associated with these minerals, we therefore should find one of the following three-phase assemblages: (A) zirconolite + baddeleyite + calzirtite, (B) zirconolite + baddeleyite + perovskite, or (C) zirconolite + calzirtite + perovskite. Assemblage (A) is known, for instance, from the carbonatite locality at Schryburt Lake, Ontario, and is feasible for Zr-rich but relatively Ca-poor portions of the system (cross-hatched area in Fig. 4); these rocks are difficult to interpret,

Tab. 5 List of zirconolite-forming reactions in the system $CaO–ZrO_2–TiO_2–CO_2$ (see Fig. 4).

1	perovskite + rutile + baddeleyite	⇔	zirconolite
2	*3* perovskite + *5* rutile + calzirtite	⇔	*5* zirconolite
3	calcite + *2* rutile + baddeleyite	⇔	zirconolite + CO_2
4	*3* calcite + *8* rutile + calzirtite	⇔	*5* zirconolite + *3* CO_2
5	calzirtite + *2* rutile	⇔	*2* zirconolite + *3* baddeleyite
6	calzirtite + *8* perovskite + *5* CO_2	⇔	*5* zirconolite + *5* calcite
7	baddeleyite + *2* perovskite + CO_2	⇔	zirconolite + calcite
8	calzirtite + CO_2	⇔	zirconolite + *4* baddeleyite + calcite

however, because both calcite and perovskite also occur.

Crystallization of zirconolite can be attributed to various processes involving solid phases, melts or fluids. Several zirconolite-forming reactions possible in this simplified system can be read from figure 4, and are listed in table 5. Alternatively, the reactions could be written in terms of CaO, ZrO_2 and TiO_2 in those cases where these components are present in a melt or a fluid rather than as solid phases. Crystallization from a silica-poor melt is one of the most important processes as documented by the numerous zirconolite occurrences in carbonatites, alkaline igneous rocks, and mesostasis areas of ultrabasic and basic rocks. Moreover, zirconolite appears to have crystallized from a melt which was produced during partial anatexis of a sapphirine granulite in Antarctica (HARLEY, 1994). Formation of zirconolite may also result from solid-melt interaction; this process has been implied, for example, to explain zirconolite rims around baddeleyite crystals which were exposed to an alnöite magma (HEAMAN and LECHEMINANT, 1993). And finally, zirconolite can be produced during metamorphism and metasomatism, i.e., by solid-solid reactions (e.g., reactions (1), (2) or (5), see Tab. 5), or by reactions involving a fluid phase. The latter mechanism, for example, led to crystallization of zirconolite in metasomatic veins at Adamello, Italy (GIERÉ, 1990; GIERÉ and WILLIAMS, 1992), and in veins and a skarn at Bergell, Switzerland/Italy (GIERÉ, 1986; RIED, 1994). At Adamello, zirconolite occurs in association with rutile and calcite, a typical assemblage for relatively Zr-poor whole-rock compositions when the prevailing physical and chemical conditions preclude formation of perovskite from calcite + rutile (Fig. 4); no relics of baddeleyite, calzirtite or perovskite have been found, and it appears that zirconolite precipitated from the fluid phase. In the Oetztal-Stubai complex, Austria, on the other hand, reaction (3) could be responsible for the growth of zirconolite rims around baddeleyite during metamorphism of carbonate rocks (PURTSCHELLER and TESSADRI, 1985).

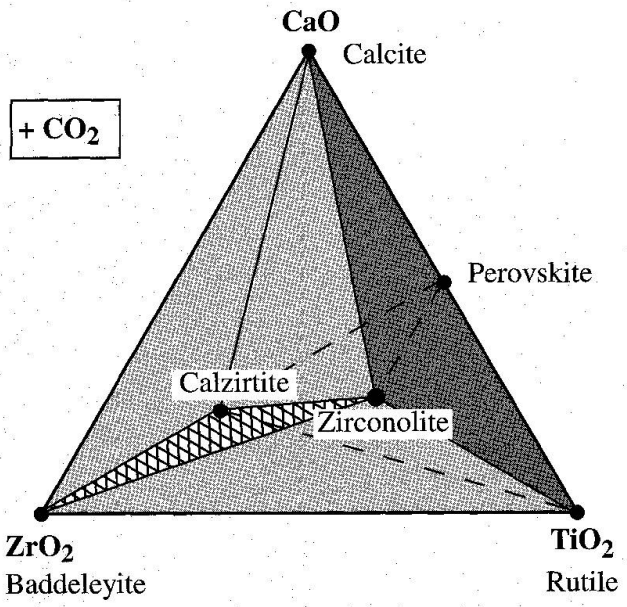

Fig. 4 Chemographic diagram for the system $CaO–ZrO_2–TiO_2–CO_2$. Cross-hatched three-phase assemblage represents an assemblage observed in the carbonatite at Schryburt Lake, Ontario. Dark-shaded field represents the assemblage found in the metasomatic veins at Adamello, Italy.

Breakdown of zirconolite, including dissolution, alteration and replacement, has also been documented. PAN (1997) provided evidence for the breakdown of zirconolite to the assemblage rutile + titanite + zircon. Dissolution (or corrosion) and alteration of zirconolite under hydrothermal conditions have been observed at several localities. At Phalaborwa, South Africa, for example, it appears that a Si-rich, S-bearing groundwater interacted with metamict zirconolite (2.05 Ga old), and alteration involved incorporation of Si along microfractures at the expense of Ca, Ti and Fe, but with Th and U remaining immobile (GIERÉ et al., 1994). At Adamello, geologically young zirconolite crystals (42 Ma old) have been corroded by an acid, reducing, P-, S-, Cl-, and F-rich fluid at $P_{total} \approx 2$ kbars and T = 500–600 °C (GIERÉ, 1996; GIERÉ and WILLIAMS, 1992); this example is the only one known to date, where release of actinides into the fluid phase is indicated.

Other examples from different geological environments include Langesundfjord (Norway), Seblyavr (Kola Peninsula, Russia), Sokli (Finland) and Cummins Range (Australia), and are currently being investigated; preliminary data indicate that a Si-bearing fluid was involved in all these cases (WILLIAMS et al., in prep.). Examples of zirconolite from Koberg, Sweden (ZAKRZEWSKI et al., 1992) and Malawi (PLATT et al., 1987) further indicate hydration of zirconolite, presumably after partial metamictization and interaction with low-temperature hydrothermal fluids; similar processes are reported for alteration of pyrochlore (LUMPKIN and EWING, 1995). Characterization of these processes, together with laboratory-based corrosion tests, are of particular importance with regard to the performance assessment of zirconolite in titanate waste forms designed for storage of high-level nuclear waste or weapons plutonium (HART et al., 1997; MALMSTRÖM et al., in press; SMITH et al., 1997).

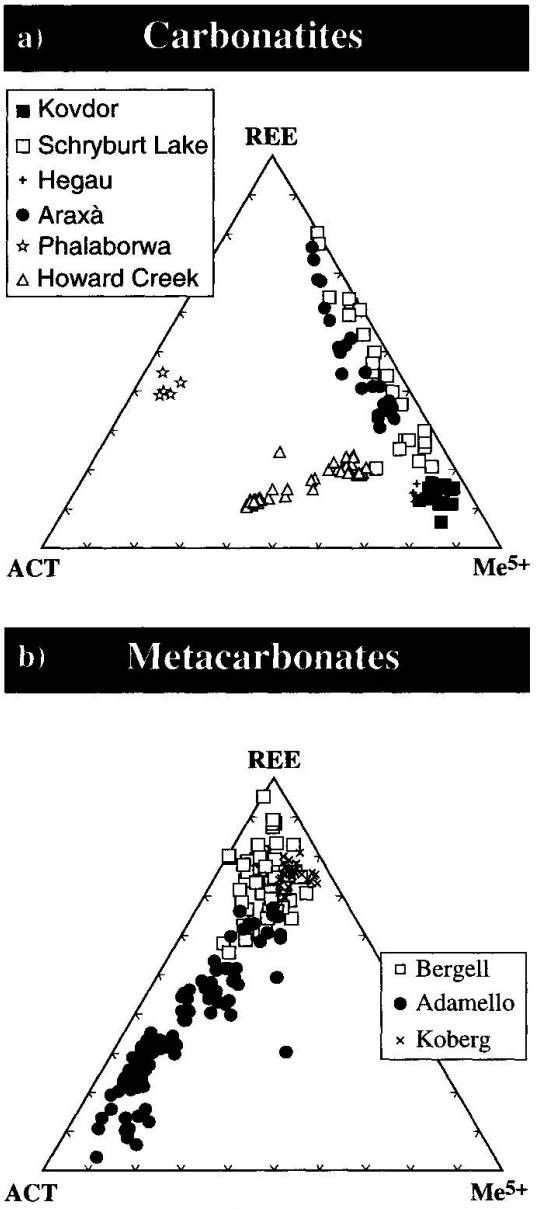

Fig. 5 Triangular plots (atomic %) showing the compositional variation of natural zirconolite with respect to REE, ACT (U+Th), and Me^{5+} (Nb+Ta) for (a) carbonatites, and (b) metacarbonates.

Compositional variation in zirconolite from various geological environments

Because of its compositional flexibility, zirconolite does not produce significant fractionation between elements of similar size/charge characteristics during its crystallization. This property leads to two distinct features which can be used as petrogenetic tools for the interpretation of zirconolite-bearing rocks: (1) The frequently observed zoning patterns record chemical changes that

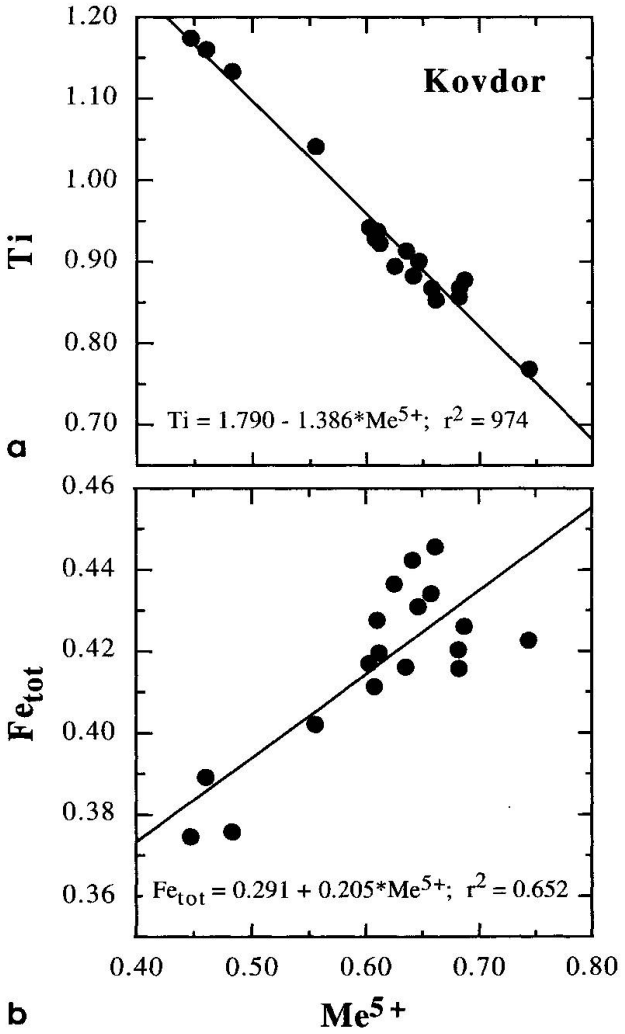

Fig. 6 Chemical variation in zirconolite from Kovdor, Russia. (a) Ti vs. Me^{5+}; (b) Fe_{tot} vs. Me^{5+} (in atoms per formula unit, based on 7 oxygens).

took place locally in the geological environment during growth, corrosion or alteration of zirconolite (GIERÉ, 1996; GIERÉ and WILLIAMS, 1992; PLATT et al., 1987; WILLIAMS and GIERÉ, 1988); and (2). The overall chemical composition of zirconolite reflects the general chemical characteristics of its geological surroundings.

The available compositional data suggest that the various chemical components can be incorporated into the zirconolite structure in more than one way, and further, that different exchange vectors operate in zirconolite from different geological environments. Here, we assess these variables, although interpretation of the analytical data for such a complex chemical system is difficult and in several cases ambiguous. In our analysis, we consider the following points: (a) correlation matrices for all important components, (b) actual ranges of the individual components, (c) slopes and intercepts of linear regressions, and (d) site totals. The statistical data for each suite of samples are given in the Appendix (Tabs A1–A9). ACT and REE were allocated to the M8 site and thus, the site total abbreviated as ΣM8 includes Ca, ACT and REE; similarly, ΣM7 includes Zr and Hf, and ΣM5,6 includes Ti and all other elements. In our procedure, we generally employ the best correlation coefficients first and use large compositional ranges only in order to assess the various substitutions (numbered as in Tab. 3). Because the valence of iron could not be determined from the EPMA data, we list the statistical data for Fe_{tot}, as well as for Me^{2+} and Me^{3+}, whereby both Me^{2+} and Me^{3+} include the *total* iron content. The oxidation state of Fe can then be inferred from the dominant substitution mechanism; it is, however, an estimate only. In the following, we discuss in some detail localities for which a large number of zirconolite analyses is available.

CARBONATITES

Zirconolite from carbonatites is highly variable with respect to the contents of REE, ACT, and Me^{5+} (Fig. 5a). This pronounced variability is, in part, the result of zirconolite having distinct compositions at individual localities: the highest Me^{5+} contents reported for zirconolite, for example, are found in a carbonatite sample from Kovdor, Russia (Tab. 1), but low concentrations are observed at Phalaborwa, South Africa (Fig. 5a). A characteristic feature of all zirconolites from carbonatites, however, is their very low Al content (≤ 0.031 Al per formula unit [p.f.u.]). Moreover, a predominance of LREE over HREE, and of Fe_{tot} over Mg is observed for all samples.

Kovdor, Russia

The niobian zirconolite from the phoscorites at Kovdor on the Kola Peninsula is rich in Fe_{tot} and Me^{5+}, thus leading to an average Ti content of less than 1 atom per formula unit (Tab. A1). It is primarily the large variation in Nb/Ti that is responsible for the pronounced zoning observed for these zirconolites in backscattered elecron (BSE) images (WILLIAMS, 1996). An excellent negative correlation is found between Ti and Me^{5+} (Fig. 6a), suggesting that substitution #2 best describes the accommodation of Me^{5+}. This indicates that Fe is present mainly as ferric iron. Substitution #5 is not consistent with the data, because Mg and Fe_{tot} correlate positively and because no other trivalent cation was detected. The linear regression of Fe_{tot} vs. Me^{5+} yields a positive slope of 0.205 (Fig. 6b) which is significantly smaller than required by substitution #2; this is due to the fact that the range in Me^{5+} is larger than that of Fe_{tot} (Tab. A1). Similarly, the range in Ti is larger than that of Me^{5+}, yielding a slope that is less negative than the one resulting from substitution #2 (Fig. 6a). Thus, an additional mechanism must exist to explain the correlated variation in Me^{5+} and Ti; this variation is possibly linked to the incorporation of REE via substitution #22, but it is difficult to assess a proper mechanism because of the effect of substitution #2 on the Me^{5+} and Ti contents. The variation in ACT, on the other hand, is fairly well constrained by the data and can be described by substitution #12. The average M5,6 totals display a slight excess which could be diminished by allowing some Mn to be accommodated on M8; this is consistent with the negative correlation found between ΣM8 and Mn (ΣM8 = 1.037–2.251*Mn; r^2 = 0.482) and with the fact that there is no correlation between Ti and M7. Incorporation of Mn^{2+} into the M8 site (up to 0.25 atoms p.f.u.) has been observed also in synthetic zirconolite (KESSON et al., 1983).

Schryburt Lake, Canada

In comparison to the Kovdor zirconolites, the crystals from this locality in Ontario are enriched in REE, but depleted in Me^{5+}, and exhibit a considerably larger range in the contents of REE, Me^{5+}, Ca, and Ti (Tab. A2). The statistical analysis reveals strong negative correlations between Ca and REE, and between Ti and Me^{5+} (Figs 7 a, b). These data are consistent with substitution #22, which is clearly the dominant substitution in these samples and best describes the observed large compositional range. Substitution #22, however, does not account for incorporation of the large

amounts of Fe (Tab. A2). The statistical data indicate that the variation in Fe is probably due to substitution #2, and thus, that Fe is present mainly as Fe^{3+}. Ferric iron therefore is the major Me^{3+}, as Cr was not detected and only very small amounts of Al are present. The variation in ACT could possibly be described by substitution #16, but the statistical data do not provide definite evidence. Although the average cation totals on each site are nearly ideal, they exhibit a considerable range (Tab. A2). The data are consistent with accommodation of some excess Zr on the M5,6 sites via substitution #1 ($\Sigma M5,6 = 2.633–0.597*Zr$; $r^2 = 0.448$).

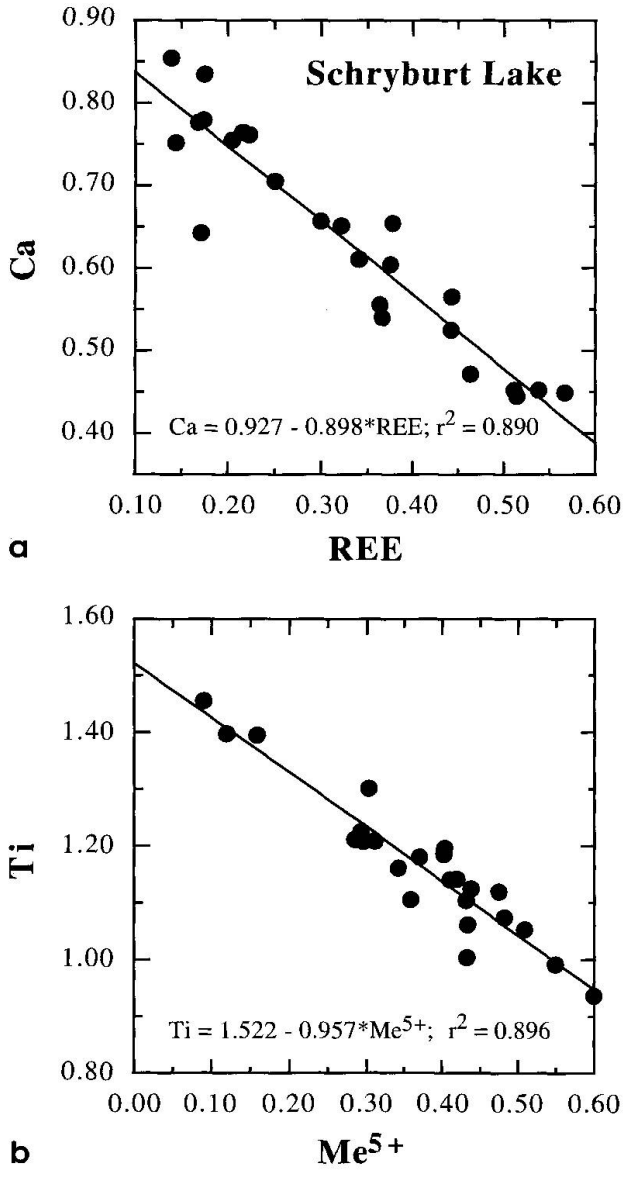

Fig. 7 Chemical variation in zirconolite from Schryburt Lake, Canada. (a) Ca vs. REE; (b) Ti vs. Me^5 (in atoms per formula unit, based on 7 oxygens).

Hegau, Germany

Zirconolite from the Hegau volcanic province exhibits large ranges in Ti and Me^{5+}, and a considerable variation in Fe_{tot}. Strong correlations are observed among several components, but only a few are significant due to low concentrations and ranges of Mg, Al, ACT and REE (Tab. A3). The statistical data reveal excellent correlations between Ti, Me^{5+} and Fe_{tot} (Fig. 8 a, b, Tab. A3); these are consistent with substitution #2, and thus with 3+ being the dominant oxidation state of Fe. Substitution #5 is also compatible with the data, however, and thus requires the presence of some bivalent Fe; substitution #5 is indicated because Fe_{tot} and (Mg + Mn) correlate positively among each other (Fig. 8c), but negatively with Al (Tab. A3). It is of note that the average Fe_{tot} content is approximately equal to that of Me^{5+}, whereas the average Al concentration is significantly lower (and Cr was not detected). These observations suggest that only a small percentage of the average Me^{5+} content could be explained in terms of substitution #5, and thus, that substitution #2 is dominant. The substitutions involving ACT and REE are difficult to assess because of the relatively low contents and ranges of these elements, and because Ca correlates poorly with both ACT and REE. Moreover, there is a positive correlation between ACT and REE which cannot be described in terms of any individual substitution listed in table 3; this trend might result from a combination of two or more substitutions such as #12, #13, #20, and #21. The Hegau zirconolites are further characterized by M7-site totals that are always larger than the theoretical value (Tab. A3). The negative correlation between $\Sigma M8$ and Zr (Fig. 8d) indicates that excess Zr may occupy the Ca site; the regression data are consistent with 2 Ca $\Leftrightarrow$ Zr + $\Diamond$, a substitution that would produce one vacancy ($\Diamond$) for each Zr on the M8 site (note, however, that the average total number of cations is 4.065, i.e. greater than the stoichiometric value[1].

Howard Creek, Canada

At this locality in British Columbia, zirconolite has high average contents of ACT and Fe_{tot}, and exhibits considerable variation in Ca, ACT and Me^{5+} (Tab. A4). The relatively good correlations observed among these components indicate that substitution #14 is dominant (Fig. 9a). This requires that Fe^{3+} is the main Me^{3+} cation involved, because the Al content is very low and Cr was not detected. There is, however, also a good inverse

correlation between ACT and REE (Fig. 9b), consistent with substitution #17. It is of note that substitutions #14 and #17 are not observed in zirconolite from any other locality (Tab. 6). This unusual correlated variation of ACT, Me^{5+} and REE is clearly visible in figure 5a, where the Howard Creek zirconolites follow a distinct trend. The M8-site totals are always smaller, the M5,6-site totals always larger than the theoretical values (Tab. A4). This could be due to accommodation of Mn^{2+}

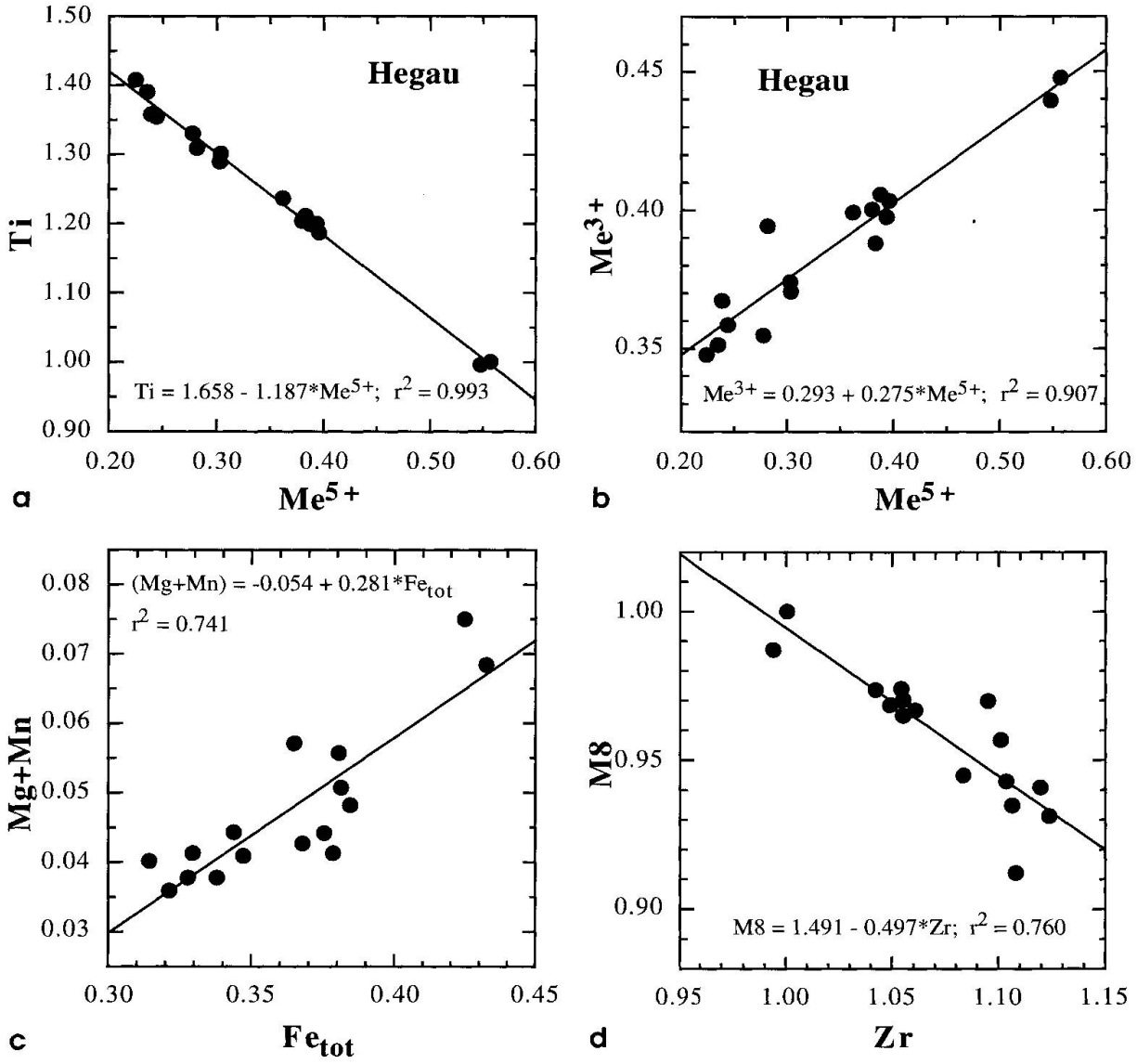

Fig. 8 Chemical variation in zirconolite from Hegau, Germany. (a) Ti vs. Me^{5+}; (b) Me^{3+} vs. Me^{5+} (total Fe included in Me^{3+}); (c) Mg+Mn vs. Fe_{tot}; (d) ΣM8 vs. Zr (in atoms per formula unit, based on 7 oxygens).

[1] Cation totals greater than 4.000 could result from the overall uncertainty associated with the data: the cumulative relative error on the cation total is estimated at 2–4% based on the count statistics for individual elements. Thus, cation totals greater than the theoretical value (but smaller than 4.160) may not be significant, and the cation totals of all analyses are smaller than 4.160. On the other hand, none of the analyses of natural zirconolite exhibit cation totals of less than 3.840, and thus vacancies are not indicated. Moreover, because the formula was calculated on the basis of O = 7.000, the cation total is dependent upon the valence of Fe and U. The latter was assumed to be present as U^{4+} in all cases, and with this assumption, the cation total is a minimum if all Fe is Fe^{3+}, but a maximum if all Fe is Fe^{2+}. The proposed vacancy-generating substitution 2 Ca ⇔ Zr + ◊ thus, is poorly constrained, particularly in Fe-rich zirconolite, and is solely indicated by the regression data for these natural zirconolites. In some synthetic zirconolites, however, vacancies have also been inferred to exist (Begg et al., 1998).

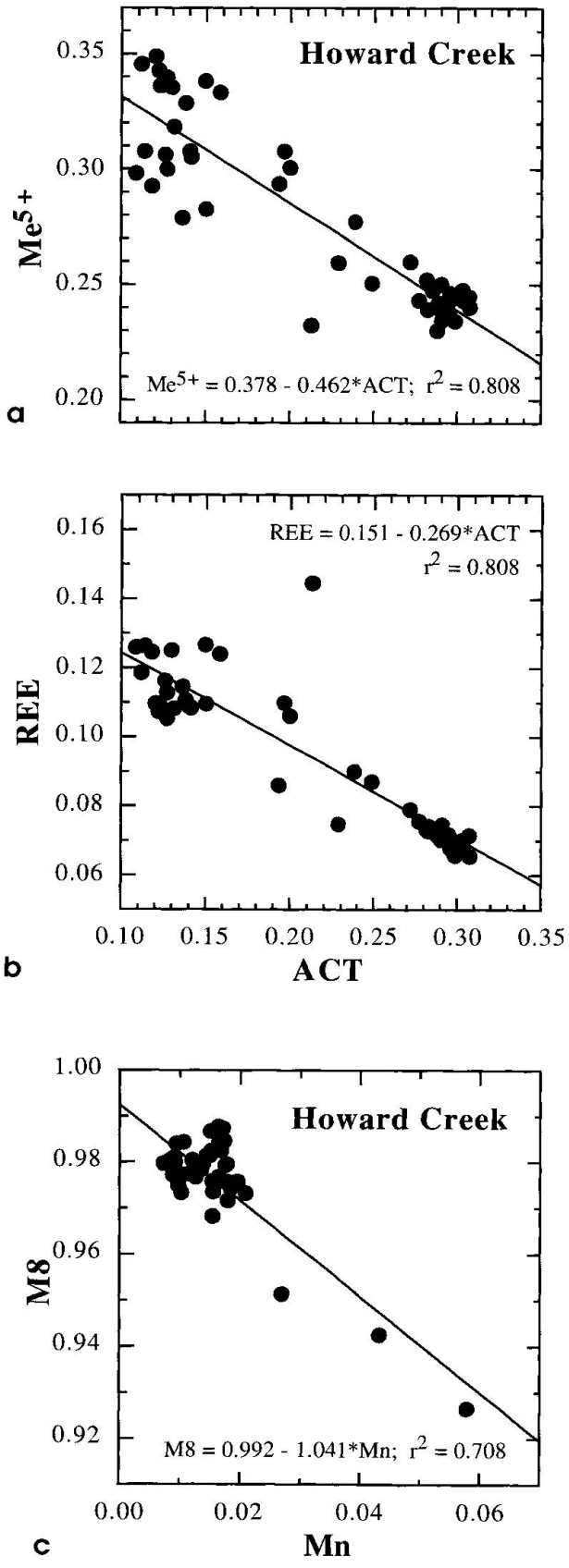

Fig. 9 Chemical variation in zirconolite from Howard Creek, Canada. (a) Me^{5+} vs. ACT; (b) REE vs. ACT; (c) ΣM8 vs. Mn (in atoms per formula unit, based on 7 oxygens).

in the M8 site rather than in the M5,6 sites; the regression data shown in figure 9c are consistent with this conclusion, although most data points cluster around the mean values of Mn and ΣM8 (0.016 and 0.976, respectively).

Araxá, Brazil

The compositional data from this carbonatite in Minas Gerais belong to two distinct populations (Fig. 10a), as suggested also by the presence of two zones that can be clearly distinguished in BSE images (C.T. WILLIAMS, unpublished data). The data set can be subdivided into an Al-bearing low-REE group and an Al-free high-REE group enriched in Fe (Fig. 10b). These two populations further exhibit different correlations among several substituting cations (Tab. A5a, A5b): a correlation between REE and Fe_{tot} and Me^{5+}, for instance, can be observed for the low-REE group but not for the high-REE group (Figs 10 b, c).

The *low-REE* zirconolite (< 0.11 REE p.f.u.) exhibits relatively large variations in Me^{5+}, Ti and Fe_{tot}, and the excellent correlations among these components suggest that substitutions #2 or #5 give rise to this variability. From the regression data shown in figure 11a, however, we conclude that #2 best describes the incorporation of Me^{5+} and Fe, and thus that Fe is present mainly as Fe^{3+}. Incorporation of the small amounts of REE is consistent with substitution #20, as indicated by the correlations between REE and Al, Fe_{tot}, and Ti (Fig. 10b, Tab. A5a). On the other hand, incorporation of REE could also be the result of substitution #21, for which there is limited evidence in figure 10c; this would require the presence of some Fe^{2+} as well. The low-REE zirconolites are further characterized by M8- and M7-site totals that are systematically low and high, respectively (Tab. A5a). Moreover, the negative correlation between ΣM8 and Zr (Fig. 11b) suggests that some Zr is accommodated in the Ca site, possibly via the exchange vector $ZrCa_{-2}$ (the average total number of cations, however, is greater than the stoichiometric value; for discussion, see footnote 1).

The *high-REE* population exhibits a significantly larger compositional variation than the low-REE group (Tab. A5b). REE and Ca exhibit identical ranges (approximately 0.16 atoms p.f.u.) and a good negative correlation (Tab. A5b, Fig. 10a). Similar relationships are exhibited by Me^{5+} and Ti, but their ranges are considerably larger (> 0.3 atoms p.f.u.). These results are consistent with substitution #22 which accounts for accommodation of all REE (Ca = 0.946–0.935*REE) but explains only about 50% of the variation in Ti

and Me^{5+}. The variation of the latter two components, however, is also correlated with that of Fe_{tot}, a feature that is best described by substitution #2. From this conclusion we infer that Fe is predominantly present as Fe^{3+}, as in the low-REE group. The data for zirconolite from Araxá clearly show that accommodation of REE at low concentration levels is achieved by a mechanism that is markedly different from that incorporating larger amounts of REE. It is of note that the existence of different exchange mechanisms is not apparent in figure 10a, where both the low- and high-REE groups plot along a line of slope –1.0, as required by substitutions #20 and #22, respectively. A distinct contrast between low-REE and high-REE zirconolite is also observed at Adamello, where the mechanism of REE incorporation

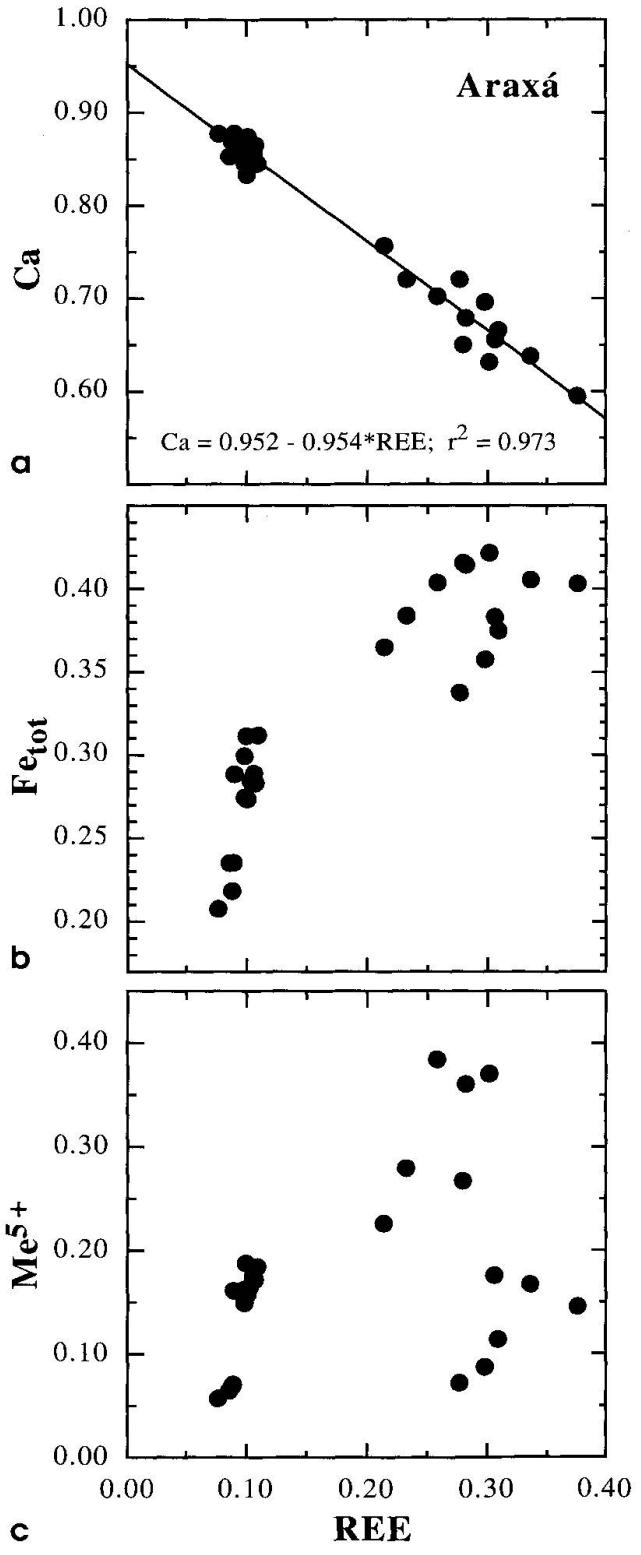

Fig. 10 Chemical variation in zirconolite from Araxá, Brazil. (a) Ca vs. REE; (b) Fe_{tot} vs. REE; (c) Me^{5+} vs. REE (in atoms per formula unit, based on 7 oxygens). Note the presence of two populations, a low-REE group and a high-REE group, in all three diagrams.

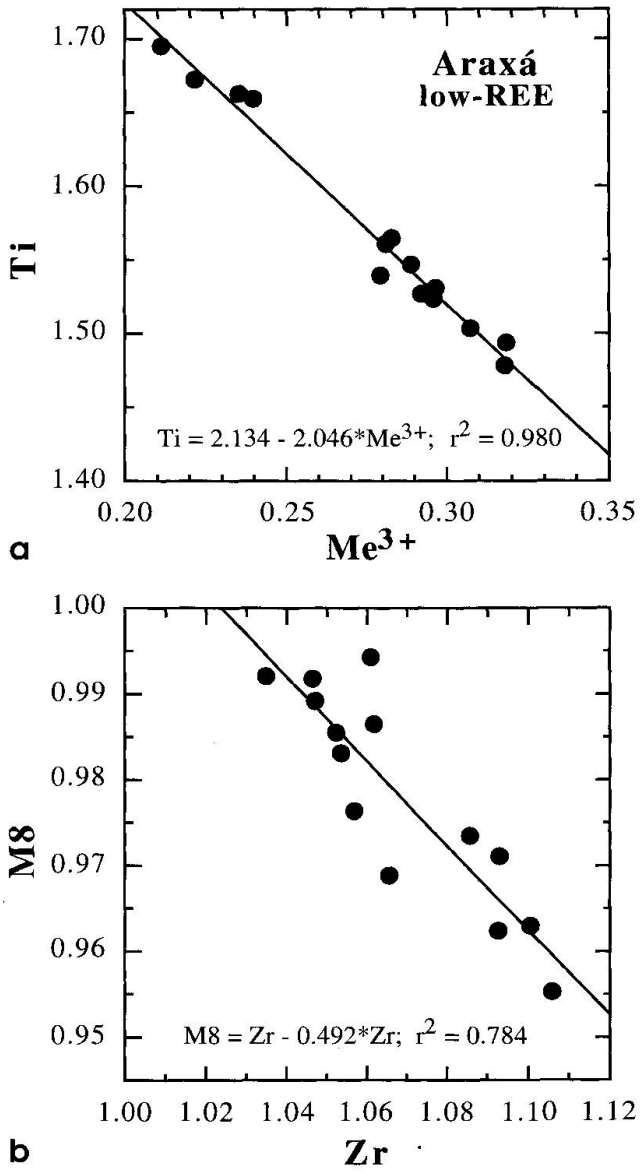

Fig. 11 Chemical variation in zirconolite from Araxá, Brazil. (a) Ti vs. Me^{3+} (total Fe included in Me^{3+}); (b) ΣM8 vs. Zr. Data for low-REE zirconolite only (in atoms per formula unit, based on 7 oxygens).

changes at very similar concentration levels (~ 0.12 REE p.f.u.; see below).

METASOMATICALLY ALTERED CARBONATE ROCKS

Zirconolite occurring in metasomatically altered carbonate rocks exhibits a very large variation in the content of ACT and is, in general, relatively poor in Me^{5+} (Fig. 5b). A considerable scatter is also observed for REE, Al, Fe_{tot} and Mg. Furthermore, there is a wide variation in REE patterns, ranging from Ce-dominated to Y-dominated compositions, a feature that is in marked contrast to zirconolite occurring in carbonatites which is always LREE-dominated. These variations result partly from zirconolite having distinctive compositions at specific localities, but also from the presence of pronounced compositional zoning within individual crystals (GIERÉ, 1990; GIERÉ and WILLIAMS, 1992; LUMPKIN et al., 1994c; WILLIAMS and GIERÉ, 1988). The presence of considerable amounts of W is a characteristic of metasomatic zirconolite occurring in metacarbonates associated with calc-alkaline intrusions (up to 1.44 wt% WO_3, see Tab. 3 in WILLIAMS and GIERÉ, 1996); in all other rock types, zirconolite contains detectable W only in a nepheline syenite at Tchivira Mt., Angola (average $WO_3 = 0.42 \pm 0.03$ wt%).

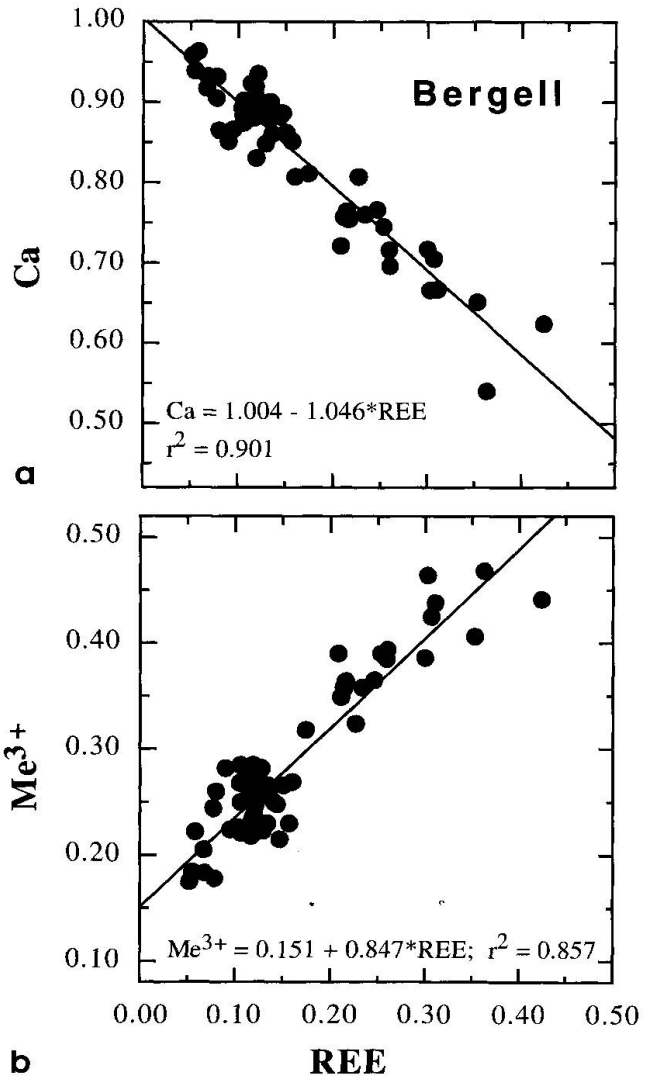

Fig. 12 Chemical variation in zirconolite from Bergell, Switzerland/Italy. (a) Ca vs. REE; (b) Me^{3+} vs. REE (total Fe included in Me^{3+}; in atoms per formula unit, based on 7 oxygens).

Bergell, Switzerland/Italy

For this example from a skarn in the Bergell contact aureole, a set of 43 analyses obtained by AEM is available in addition to the 15 EPMA data of WILLIAMS and GIERÉ (1996). There is an excellent agreement between the two data sets (LUMPKIN et al., 1994c), and thus a combined data set is used in the following discussion. There is no evidence for a distinct low-REE and high-REE population, as a continuous compositional variation is found from 0.052 to 0.424 atoms per formula unit (Fig. 12a). Moreover, if we subdivide the data into a low-REE and high-REE data set (transition at 0.12 REE p.f.u., see above), the statistical parameters are nearly identical in both sets, and thus there is no evidence in this case for a significant difference in the behavior of REE at different concentration levels. Therefore, the statistical parameters are presented for the entire data set (Tab. A6a). As pointed out by WILLIAMS and GIERÉ (1988) and LUMPKIN et al. (1994c), the dominant exchange mechanism in this sample is substitution #20, requiring that most of the Fe is trivalent (Fig. 12b). Substitution #12 is also indicated by the data ($Me^{2+} = 0.166 + 2.418$*ACT; $r^2 = 0.767$), but is of lesser importance because the range in ACT is considerably smaller than that of REE (0.117 vs. 0.372 atoms p.f.u.). A slope of +2.43 was obtained from the linear regression of REE vs. ACT and provides an estimate for the relative magnitudes of substitutions #20 and #12; the predominance of substitution #20 is clearly visible also in figure 15b (see below). The chemical analyses exhibit generally an excess of cations on the M8 site, and often a slight deficit on the M7 site. This observation indicates that some REE or ACT substitute for Zr on the M7 site (see also LUMPKIN et al., 1994c). To test this hypothesis, we calculated linear regressions for ΣM7 vs. REE and ACT. The data, shown in table A6b, are consistent with the above hypothesis, but reveal that it must be refined in order to explain the pronounced dif-

ferences observed between U and Th as well as among individual REE. The least squares fit for U, for example, is better than that for Th, suggesting that U is more likely to substitute for Zr. Similarly, ΣM7 exhibits a fairly strong inverse correlation with most of the heavy REE, but not with La, Ce, Pr, and Nd. This marked contrast is clearly reflected by the significantly different correlations observed for LREE and HREE. The statistical analysis, even though not complete because some REE were not detectable in all cases (Tab. A6b), thus suggests that the M7 site is partly occupied by U, HREE and possibly Y; on this site, however, these elements do not account for more than approximately 0.05–0.10 atoms per formula unit. U enters the Zr site via the simple substitution #8; accommodation of REE is more complex because of charge balance requirements, and could be achieved via substitutions #24 or #9 (or both).

Adamello, Italy

Two samples from a Ti-rich vein in a contact metamorphic marble have been studied in detail by GIERÉ and WILLIAMS (1992) who reported that there was a distinct difference in the behavior of REE at low and high concentration levels (transition at ~ 0.12 REE p.f.u., corresponding to approximately 5 wt% REE_2O_3). More data are available now because an additional sample has been studied by AEM in order to characterize radiation damage effects (LUMPKIN et al., 1997). Because it has been shown that analyses obtained for zirconolite by AEM agree very well with those obtained by EPMA (LUMPKIN et al., 1994c), we included the AEM data into this discussion and thus have access to a significantly larger database. The large ranges in most chemical components, particularly in ACT and REE, make the Adamello zirconolites especially valuable in view of deducing the most important substitutions. The new data set confirms the conclusion of GIERÉ and WILLIAMS (1992) that the REE-involving substitution in low-REE zirconolite is different from that in high-REE zirconolite (#20 and #21, respectively).

Low-REE zirconolite: The excellent correlations among Ca, ACT, Ti and Me^{2+} (Tab. A7a) and the diagram shown in figure 13a confirm that substitution #12 is responsible for incorporation of ACT, and thus that Fe is mostly bivalent. It is of note that up to 0.475 ACT per formula unit (the highest reported ACT content; cf. Tab. 1) are accommodated via substitution #12 (Fig. 13a). The correlation between Al and REE has been improved only very slightly in comparison to the original data set, but it is consistent with substitution #20.

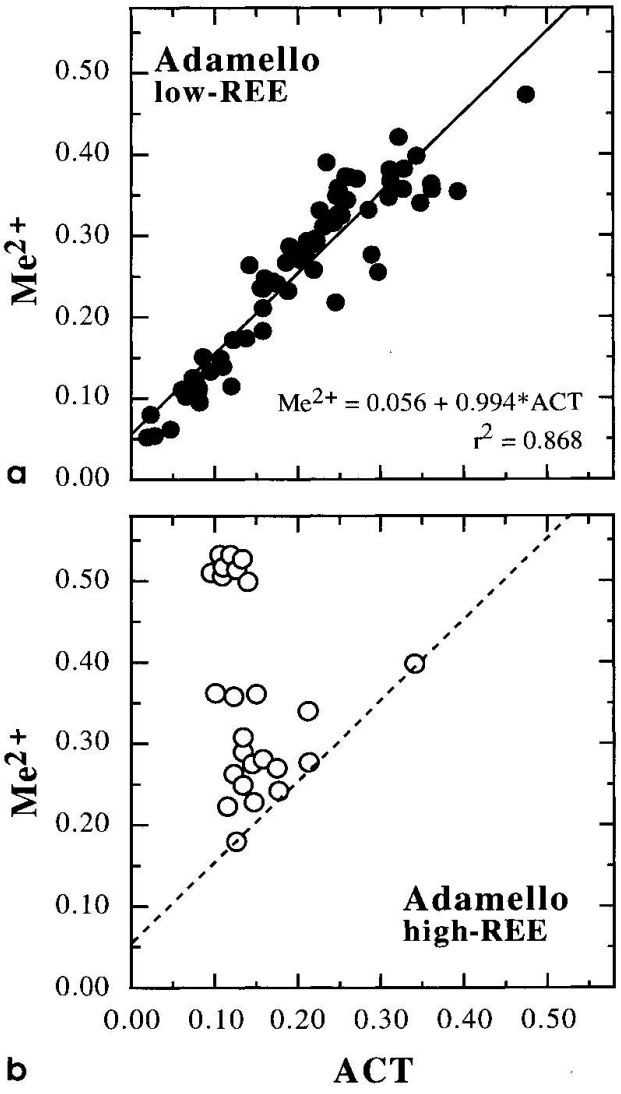

Fig. 13 Variation of Me^{2+} and ACT in zirconolite from Adamello, Italy (total Fe included in Me^{2+}). (a) low-REE group; (b) high-REE group (in atoms per formula unit, based on 7 oxygens). For comparison, the regression line obtained for the low-REE data set (solid line in Fig. 13a) is also plotted in the diagram for the high-REE zirconolite (dashed line in Fig. 13b); see text for discussion.

High-REE zirconolite: The observed correlations among the major components are significantly less good than those exhibited by the low-REE zirconolite because of complex interferences between different substitutions (Tab. A7b). Although ACT are most likely incorporated via substitution #12, the trend is not evident in figure 13b. As pointed out by GIERÉ and WILLIAMS (1992), this is the result of Fe^{2+} being involved in a second exchange mechanism, namely substitution #21. This interpretation provides an explanation why almost all data points plot above the dashed

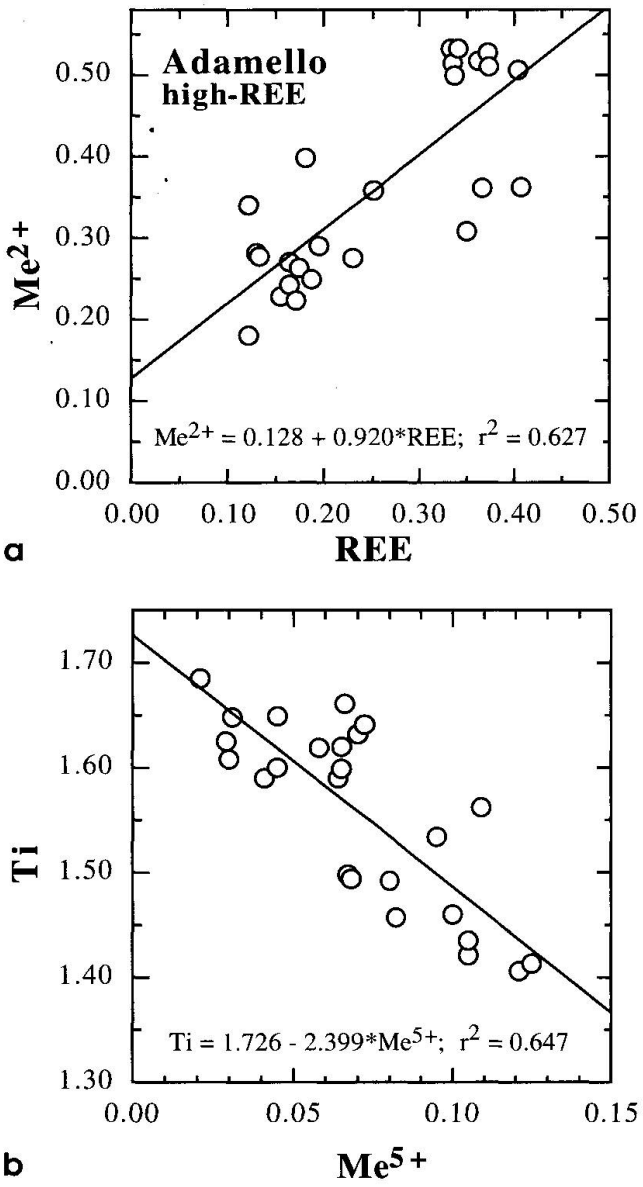

Fig. 14 Chemical variation in zirconolite from Adamello, Italy. (a) Me^{2+} vs. REE (total Fe included in Me^{2+}); (b) Ti vs. Me^{5+}. Data for high-REE zirconolite only (in atoms per formula unit, based on 7 oxygens).

line of slope +1 in figure 13b, and is also consistent with the data listed in table A7b and the linear regression shown in figures 14 a and b. The larger data set available for the present study further allows to substantiate the hypothesis of GIERÉ and WILLIAMS (1992) that some ACT or heavy REE may substitute for Zr on the M7 site: the latter exhibits slight deficiencies in all cases, whereas M8-site totals are always too high (Tab. A7b). Moreover, weak inverse correlations are observed between ΣM7 and ACT (slope = –0.299, r^2 = 0.130) and between ΣM7 and REE (slope = –0.157, r^2 = 0.147); although very poor, these correlations are consistent with the above hypothesis and possibly with substitutions #8 and #9 or #11. It is of note that at Adamello, the correlations between ΣM7 and ACT and REE are considerably weaker than at Bergell (Tab. A6b); this observation is generally also valid for individual REE, and U and Th.

Koberg, Sweden

This sample from the Bergslagen ore district is characterized by relatively high average contents of Mn (0.05 Mn p.f.u.), REE and Fe_{tot}. It further exhibits a large variation in Fe_{tot} and a fairly large range in Ca, REE, Ti and Mg. Inspection of table A8, however, reveals no strong correlations among these components. In spite of this, the data are consistent with substitution #20 which would account for all the variation in REE and nearly the entire variability in Ti and Ca. Substitution #20 would further infer that Fe is mostly trivalent; this conclusion, however, appears to be in contrast with the petrographic observations which revealed that zirconolite is closely associated with sulfides. The strong positive correlation between Mg and Al points to a substitution relating the exchange of Me^{2+} and Me^{3+} on the M5,6 sites (e.g., Mg + Al ⇔ Mn^{2+} + Fe^{3+}), but the data do not allow us to verify this mechanism.

NEPHELINE SYENITES

At present, the data set for zirconolite occurring in other terrestrial rock types is very limited (Tab. 4) and consequently, a statistical evaluation is not feasible. A considerable number of analyses, however, is available for nepheline syenites. In these host rocks, zirconolite is often rich in Fe, but poor in Al and Mg, as observed, for example, on Chilwa Island in southern Malawi and at Tre Croci in Latium, Italy (WILLIAMS and GIERÉ, 1996). In strong contrast to these findings, zirconolite at Tchivira Mt., an alkaline complex near Quilengues in southern Angola, has extremely low Fe contents and the highest reported concentrations of Al and Mg (Al_2O_3 = 3.43 wt%, MgO = 3.53 wt%; see Tab. 1). Even though only six single-spot analyses are available for the Tchivira Mt. zirconolite, the data indicate that some Mg is accommodated in the M8 site; this conclusion is consistent with systematically low M8-site totals (ΣM8 = 0.841 ± 0.027) and high M5,6-site totals (ΣM5,6 = 2.136 ± 0.044; data from WILLIAMS and GIERÉ, 1996). The Mg-rich zirconolite from Tchivira Mt. is the only sample that provides evidence for the substitution Ca ⇔ Mg, which also

Tab. 6 Substitutions operating in zirconolite from various localities.

Rock type	Locality	Substitution # dominant	Substitution # others	Type of zirconolite [1]	Inferred main valence of iron
Carbonatite	Kovdor, Russia	2	12, 22(?), $MnCa_{-1}$	low-REE [2]	3+
	Schryburt Lake, Canada	22, 2	16(?), 1(?)	high-REE	3+
	Hegau, Germany	2	5, $ZrCa_{-2}$(?)	low-REE	3+, (2+)
	Howard Creek, Canada	14	17, $MnCa_{-1}$	low-REE [2]	3+
	Araxá, Brasil	2	20, 21(?), $ZrCa_{-2}$(?)	low-REE	3+
		22, 2		high-REE	3+
Metacarbonate	Bergell, Switzerland-Italy	20	12, 8, 24/9(?)	low/high [3]	3+, (2+)
	Adamello, Italy	12, 20		low-REE	2+
		12, 21	8, 9/11(?)	high-REE	2+
	Koberg, Sweden	20		high-REE	3+, 2+ (?)
Lunar basalt	Various landing sites	23, 20	1, $ZrCa_{-2}$(?)	high-REE	2+, 3+

[1] Definition of "low-REE": ΣREE is less than approximately 0.12 atoms per formula unit. ΣREE = 0.1 corresponds to approximately 5 wt% REE_2O_3

[2] Most analyses have ΣREE ≤ 0.12 atoms per formula unit

[3] Same substitutions are operating in both low-REE and high-REE zirconolite

has not been observed in synthetic samples. It remains to be studied whether this unusual zirconolite composition is due to a peculiar host-rock composition.

LUNAR BASALTS

Most lunar zirconolites were found in basaltic rocks. These zirconolites are very rich in REE (highest REE content reported for natural samples: REE_2O_3 = 31.98 wt%, cf. Tab. 1), always HREE-dominated and, on average, significantly richer in Hf and Zr (average contents in atoms p.f.u.: Hf = 0.014 ± 0.009; Zr = 1.141 ± 0.134) than those occurring in other host rocks. The samples from lunar basalts are further characterized by generally high Cr and Fe contents whereby Fe_{tot} invariably predominates over Mg. In contrast, they contain only small amounts of Nb and Ta, and little or no ACT, a feature that is consistent with their basaltic host rocks.

Table A9 shows that zirconolite from lunar basalts exhibits very large ranges in Ca and REE, and varies considerably with respect to Fe_{tot} and Ti. The statistical parameters indicate that the dominant substitution in lunar basalts is probably #23. Substitution #20, however, appears to be important also, as suggested by the relatively large range in Ti. If substitutions #20 and #23 are both responsible for the incorporation of the large amounts of REE, iron must be present as Fe^{2+} and Fe^{3+}. The average M8-site totals are generally lower, the M7-site totals systematically higher than the theoretical values, suggesting that some Zr is accommodated in the Ca site; the statistical data are consistent with this conclusion and point to the substitution Zr + ◊ ⇔ 2 Ca. The extent of this substitution, however, is limited and the correlation between the M8-site totals and Zr is weak (ΣM8 = 1.567–0.610*Zr; r^2 = 0.269); moreover, the average total number of cations is nearly stoichiometric (ΣM = 4.032). The M5,6-site totals exhibit a very large variation and the data indicate that some Zr may additionally be accommodated on M5,6 via substitution #1 (ΣM5,6 = 2.611–0.531*Zr; r^2 = 0.317). Zirconolite from lunar basalts thus provides some evidence for the presence of Zr on the M8 and M5,6 sites, in addition to the M7 site.

Discussion

The preceding evaluation of the compositional variation in zirconolite from various geological settings is summarized in table 6. The latter reveals that only a few of the substitutions listed in table 3 are important in natural zirconolite, i.e. substitutions #2, #12, #20, and #22. Moreover, the inferred predominant oxidation state of Fe is in many cases trivalent, as expected in these geological environments. Ferrous iron appears to be important only at Adamello, where reducing conditions during zirconolite crystallization have been documented (GIERÉ, 1996).

Table 6 further shows that substitutions #12 and #20 are typical for zirconolite from metacarbonates, whereas substitutions #2 and #22 are characteristic for carbonatitic environments. This means that most natural zirconolites will plot in the upper part of the composition space shown in figure 3, above the shaded plane. The latter can be

used to display the compositions and trends of zirconolite in metacarbonates, whereas the plane delimited by substitutions #2, #20, and #22 is most convenient for displaying ACT-poor zirconolite from carbonatites (see Fig. 15). These diagrams further allow to distinguish between low- and high-REE samples as well as between Me^{2+}- and Me^{3+}-dominated compositions.

These results clearly show that large amounts of Me^{5+} most commonly enter the zirconolite structure via substitution #2. This is particularly well displayed by the low-REE zirconolites from Kovdor, Hegau and Araxá (see Fig. 15a). Incorporation of Me^{5+} is inversely correlated with that of REE in geochemical environments where both elements are available in relatively high concentrations: this is documented by the predominance of substitution #22 in the high-REE zirconolites from carbonatite complexes (Tab. 6).

Inspection of table 6 further reveals that at low concentration levels (i.e. < 0.12 REE p.f.u.), the REE are most commonly accommodated via substitution #20; at higher levels, substitution #20 is only observed in relatively oxidizing and/or Me^{5+}-poor geochemical environments such as in the Bergell skarn and lunar basalts (the situation at Koberg is less clear, see above). In reducing environments, however, accommodation of substantial quantities of REE seems to be possible only if considerable amounts of Me^{5+} are available, as indicated by the Adamello high-REE zirconolites (substitution #21). These observations may offer an explanation why different trends are observed for low- and high-REE zirconolite at Adamello, but not at Bergell.

The most important mechanism by which large amounts of ACT (up to 0.475 ACT p.f.u.) are incorporated into the zirconolite structure is substitution #12, which requires the presence of a charge-balancing bivalent metal cation. The low-REE-zirconolites from Adamello exemplify this trend in figures 13a and 15b. If a bivalent cation is not available in sufficient quantities, other substitutions are involved; this is documented, for example, by zirconolite from the Howard Creek carbonatite, where accommodation of ACT is correlated with that of Me^{5+} via substitution #14 (Fig. 9a); the data for this sample plot in the interior part of the double tetrahedron (Fig. 3) and thus, are not plotted in figure 15a.

The data shown in table 6 indicate that Zr may in some cases be present on sites other than M7. The strongest evidence for Zr on the M8 site is provided by the low-REE zirconolites from Araxá (Fig. 11b) and those from Hegau (Fig. 8d), whereas best evidence for Zr on the M5,6 sites is provided by the lunar samples; the substitution

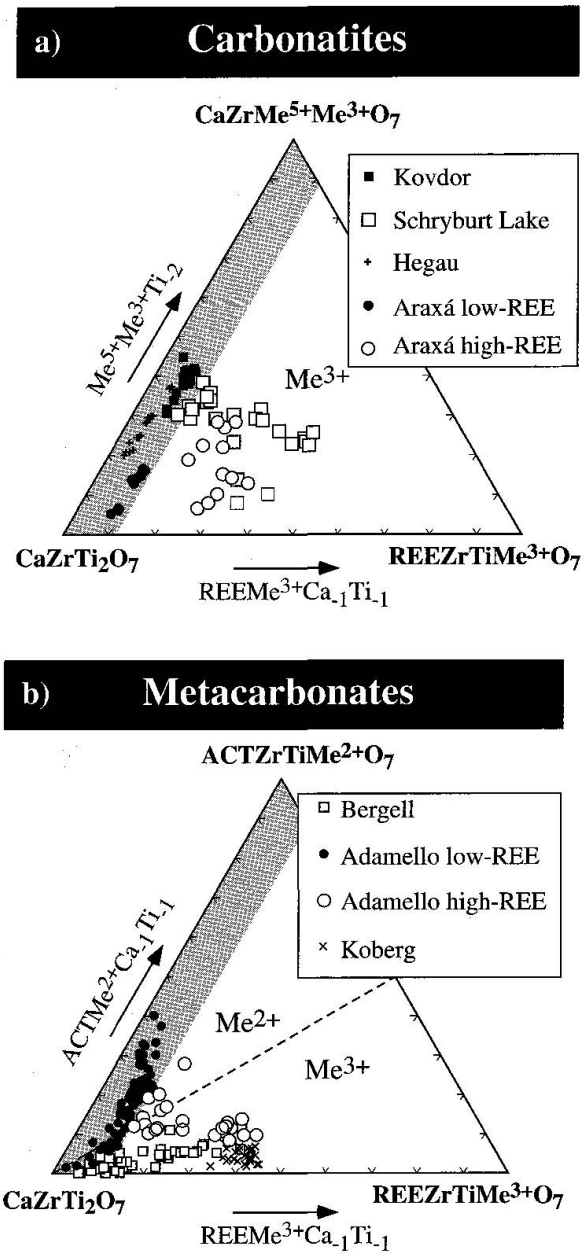

Fig. 15 Triangular plots displaying the composition of zirconolite from selected suites of samples. (a) zirconolite from carbonatites shown in the diagram $CaZrTi_2O_7$ – $REEZrTiMe^{3+}O_7$ – $CaZrMe^{5+}Me^{3+}O_7$ (represents the plane delimited by substitutions #2, #20, and #22 in Fig. 3; the entire plane is thus located in the Me^{3+}-dominated part of the double tetrahedron shown in Fig. 3). Note the distinction between low-REE and high-REE zirconolite from Araxá. (b) zirconolite from metasomatically altered carbonate rocks shown in the diagram $CaZrTi_2O_7$ – $REEZrTiMe^{3+}O_7$ – $ACTZrTiMe^{2+}O_7$ (represents shaded plane in Fig. 3). Dashed line divides the triangle into a Me^{2+}-dominated ACT-rich part (upper left) and a Me^{3+}-dominated REE-rich part (lower right). Note the distinction between low-REE and high-REE zirconolite from Adamello. The shaded area represents in both diagrams the composition of low-REE zirconolite. The data were plotted by using the number of Ca, REE, ACT and Me^{5+} atoms per formula unit (based on 7 oxygens).

mechanisms can be described as $Zr + \Diamond \Leftrightarrow 2\,Ca$ (although there is no direct indication of vacancies, see footnote 1) and $Zr \Leftrightarrow Ti$, respectively. There is no evidence for these substitutions in metacarbonates (cf. Tab. 6). It is of note that the zirconolites from both the Araxá carbonatite and the lunar basalts are richer in Hf than any other sample (max. HfO_2 = 1.34 wt%), suggesting that the M8 and M5,6 sites may also accommodate some Hf in addition to Zr. This hypothesis seems justified because the ionic radius of Hf^{4+} is only slightly smaller than that of Zr^{4+} ($^{[8]}Hf^{4+}$ = 0.83 Å, $^{[8]}Zr^{4+}$ = 0.84 Å; SHANNON, 1976). The concentration of Hf, however, is in both samples too low (~ 0.014 Hf p.f.u.) to test the hypothesis.

Our results suggest that the redox conditions prevailing at the time of zirconolite crystallization exert a significant control on the substitution mechanisms, and possibly on the total amounts of REE and ACT accommodated by zirconolite. Moreover, natural zirconolite most often occurs in SiO_2-undersaturated rocks and therefore, the silica activity probably plays an important role in the distribution of zirconolite. This indicates that SiO_2-bearing fluids may react with and thus destabilize zirconolite. The limited number of important substitutions observed in natural zirconolite indicates that these substitutions probably produce energetically more favorable (stable) compositions. This would imply that high-level nuclear waste elements should be incorporated into synthetic zirconolite in a similar way to that observed in natural samples.

Acknowledgements

The authors are grateful to Drs. G. Bayer (ETH Zürich), B. Grobéty (Århus Universitet) and L. Hecht (CREGU, Nancy) for their critical and thorough reviews. We further would like to express our sincere gratitude to Drs. G. Bayer, J.B. Dawson, E.S. Grew, S.L. Harley, I. Hornig-Kjarsgaard, J. Keller, A.O. Larsen, A.N. Mariano, G.C. Parodi, R.G. Platt, and to the Kovdor Mining Museum (Kola Peninsula, Russia) for providing us with zirconolite samples and/or for allowing us to include unpublished data. We thank Drs. K.L. Smith and E.R. Vance (both at ANSTO, Australia) for helpful comments and fruitful discussions, and Dr. J. Brugger (Universität Basel) for drawing the crystal structure of zirconolite (using the computer program "ATOMS", ©1991 Eric Dowty, Kingsport, TN 37663, USA).

References

ALLEN, C.M. and ELLIS, D.J. (1996): A theoretical analysis of the stability and phase relations involving zirconolite in the CaO–ZrO_2–TiO_2–SiO_2–CO_2 system under crustal and upper mantle conditions. A report for ANSTO. Department of Geology, Faculty of Science, The Australian National University, Canberra, ACT.

BAYLISS, P., MAZZI, F., MUNNO, R. and WHITE, T.J. (1989): Mineral nomenclature: zirconolite. Mineral. Mag. 53, 565–569.

BEGG, B.D. and VANCE, E.R. (1997): The incorporation of cerium in zirconolite. In: GRAY, W.J. and TRIAY, I.R. (eds): Scientific Basis for Nuclear Waste Management XX, 465, p. 333–340. Materials Research Society, Boston, USA.

BEGG, B.D., VANCE, E.R. and LUMPKIN, G.R. (1998): Charge compensation and the incorporation of cerium in zirconolite and perovskite. In: MCKINLEY, I.G. and MCCOMBIE, C. (eds): Scientific Basis for Nuclear Waste Management XXI, 506, p. 79–86. Materials Research Society, Davos, Switzerland.

BUCK, E. and GIERÉ, R. (in press): Intergrowth structures in synthetic pyrochlores: Implications for radiation damage effects and waste form formulation. Ed. Scientific Basis for Nuclear Waste Management XXII. Materials Research Society, Boston, USA.

CABELLA, R. and GAZZOTTI, M. (1994): Ti–Zr-rich oxides in "chromitite" layers from the Bracco ophiolite complex (Eastern Liguria, Italy). International Mineralogical Association, 16th General Meeting, Abstract Volume 16, p. 60–61, Pisa, Italy.

CHEARY, R.W. and COELHO, A.A. (1997): A site occupancy analysis of zirconolite $CaZr_xTi_{3-x}O_7$. Phys. Chem. Minerals 24, 447–454.

COELHO, A.A., CHEARY, R.W. and SMITH, K.L. (1997): Analysis and Structural Determination of Nd-substituted zirconolite-4M. J. Solid State Chem. 129, 346–359.

D'OREY, F.L.C. (1991): Optical and physical characteristics of a niobium-rich zirconolite from Cape Verde. Garcia de Orta, Série de Geologia 14(1–2), 7–8.

DE HOOG, J.C.M. and VAN BERGEN, M.J. (1996): Zirconolite in K-rich calc-alkaline lavas from Lewotolo Volcano (E. Indonesia): Late-stage mobility of HFSE and REE in arc magmas. V.M. Goldschmidt Conference, 1(1), p. 122. Cambridge Publications, Heidelberg, Germany.

DE HOOG, J.C.M. and VAN BERGEN, M.J. (1997): Notes on the chemical composition of zirconolite with thorutite inclusions from Walaweduwa, Sri Lanka. Mineral. Mag. 61, 721–725.

FIELDING, P.E. and WHITE, T.J. (1987): Crystal chemical incorporation of high level waste species in aluminotitanate-based ceramics: Valence, location, radiation damage, and hydrothermal durability. J. Mater. Res. 2(3), 387–414.

GATEHOUSE, B.M., GREY, I.E., HILL, R.J. and ROSSELL, H.J. (1981): Zirconolite, $CaZr_xTi_{3-x}O_7$; structure refinements for near-end-member compositions with x = 0.85 and 1.30. Acta Cryst. B37, 306–312.

GIERÉ, R. (1986): Zirconolite, allanite and hoegbomite in a marble skarn from the Bergell contact aureole: implications for mobility of Ti, Zr and REE. Contrib. Mineral. Petrol. 93, 459–470.

GIERÉ, R. (1990): Quantification of element mobility at a tonalite/dolomite contact (Adamello Massif, Provincia di Trento, Italy). Ph. D. thesis, ETH Zürich, Switzerland, p. 250.

GIERÉ, R. (1996): Formation of rare earth minerals in hydrothermal systems. In: JONES, A.P., WALL, F. and WILLIAMS, C.T. (eds): Rare Earth Minerals: Chemistry, origin and ore deposits. Chapman & Hall, London: 105–150.

GIERÉ, R., GUGGENHEIM, R., DÜGGELIN, M., MATHYS, D., WILLIAMS, C.T., LUMPKIN, K.L., BLACKFORD,

M.G., HART, K.P. and MCGLINN, P. (1994): Retention of actinides during alteration of aperiodic zirconolite. 13th International Congress on Electron Microscopy, Applications in Materials Sciences 2B, p. 1269–1270, Paris.

GIERÉ, R. and WILLIAMS, C.T. (1992): REE-bearing minerals in a Ti-rich vein from the Adamello contact aureole (Italy). Contrib. Mineral. Petrol. 112, 83–100.

HARDING, R.R., MERRIMAN, R.J. and NANCARROW, P.H.A. (1982): A note on the occurrence of chevkinite, allanite, and zirkelite on St. Kilda, Scotland. Mineral. Mag. 46, 445–448.

HARLEY, S.L. (1994): Mg–Al yttrian zirconolite in a partially melted sapphirine granulite, Vestfold Hills, East Antarctica. Mineral. Mag. 58, 259–269.

HART, K.P., LUMPKIN, G.R., ELLIS, D.J., ALLEN, C.M., GIERÉ, R., WILLIAMS, C.T. and VANCE, E.R. (1997): Further analysis of the applicability of naturally occurring zirconolites as analogues for HLW waste matrices. In: VON MARAVIC, H. and SMELLIE, J. (eds): 7th EC Natural Analogue Working Group Meeting, Report EU17851, p. 3–8. European Commission, Stein am Rhein, Switzerland.

HEAMAN, L.M. and LECHEMINANT, A.N. (1993): Paragenesis and U–Pb systematics of baddeleyite (ZrO_2). Chem. Geol. 110, 95–126.

KESSON, S.E., SINCLAIR, W.J. and RINGWOOD, A.E. (1983): Solid solution limits in Synroc zirconolite. Nuclear and Chemical Waste Management 4, 259–265.

LAVEROV, N.P., OMEL'YANENKO, B.I., YUDINTSEV, S.V. and NIKONOV, B.S. (1996): Zirconolite as a Matrix for Immobilization of High-Level Radioactive Wastes. Geology of Ore Deposits 38(5), 345–352.

LUMPKIN, G.R. and EWING, R.C. (1995): Geochemical alteration of pyrochlore group minerals: Pyrochlore subgroup. Am. Mineral. 80, 732–743.

LUMPKIN, G.R., HART, K.P., MCGLINN, P.J., PAYNE, T.E., GIERÉ, R. and WILLIAMS, C.T. (1994a): Retention of actinides in natural pyrochlores and zirconolites. Radiochimica Acta 66/67, 469–474.

LUMPKIN, G.R., SMITH, K.L. and BLACKFORD, M.G. (1991): Electron microscope study of Synroc before and after exposure to aqueous solutions. J. Mater. Res. 6(10), 2218–2233.

LUMPKIN, G.R., SMITH, K.L. and BLACKFORD, M.G. (1995): Partitioning of uranium and rare earth elements in Synroc: effect of impurities, metal additive, and waste loading. J. Nucl. Mater. 224, 31–42.

LUMPKIN, G.R., SMITH, K.L., BLACKFORD, M.G., GIERÉ, R. and WILLIAMS, C.T. (1998): The crystalline-amorphous transformation in natural zirconolite: evidence for long-term annealing. In: MCKINLEY, I.G. and MCCOMBIE, C. (eds): Scientific Basis for Nuclear Waste Management XXI, 506, p. 215–222. Materials Research Society, Davos, Switzerland.

LUMPKIN, G.R., SMITH, K.L., BLACKFORD, M.G., HART, K.P., MCGLINN, P., GIERÉ, R. and WILLIAMS, C.T. (1994b): Prediction of the long-term performance of crystalline nuclear waste form phases from studies of mineral analogues. In: MCDONALD, N.R. (ed.): 9th Pacific Basin Nuclear Conference, 94/6, p. 879–885. The Institution of Engineers, Sydney, Australia.

LUMPKIN, G.R., SMITH, K.L. and GIERÉ, R. (1997): Application of analytical electron microscopy to the study of radiation damage in natural zirconolite. Micron 28, 57–68.

LUMPKIN, G.R., SMITH, K.L., M.G., B., GIERÉ, R. and WILLIAMS, C.T. (1994c): Determination of 25 elements in the complex oxide mineral zirconolite by analytical electron microscopy. Micron 25(6), 581–587.

MALMSTRÖM, J., REUSSER, E., GIERÉ, R., LUMPKIN, G., GUGGENHEIM, R., DUEGGELIN, M. and MATHYS, D. (in press): Zirconolite corrosion in dilute acid and basic fluids at 180–700 °C and 50 MPa. Scientific Basis for Nuclear Waste Management XXII. Materials Research Society, Boston, MA.

MAZZI, F. and MUNNO, R. (1983): Calciobetafite (new mineral of the pyrochlore group) and related minerals from Campi Flegrei, Italy; crystal structures of polymignyte and zirkelite: comparison with pyrochlore and zirconolite. Am. Mineral. 68, 262–276.

PAN, Y. (1997): Zircon- and monazite-forming metamorphic reactions at Manitouwadge, Ontario. Can. Mineral. 35, 105–118.

PLATT, R.G., WALL, F., WILLIAMS, C.T. and WOOLLEY, A.R. (1987): Zirconolite, chevkinite and other rare earth minerals from nepheline syenites and peralkaline granites and syenites of the Chilwa Alkaline Province, Malawi. Mineral. Mag. 51, 253–263.

PURTSCHELLER, F. and TESSADRI, R. (1985): Zirconolite and baddeleyite from metacarbonates of the Oetztal-Stubai complex (northern Tyrol, Austria). Mineral. Mag. 49, 523–529.

PYATENKO, Y.A. and PUDOVKINA, Z.V. (1964): The lattice metric of $CaZrTi_2O_7$ crystals. Kristallografiya 9, 98–100.

RIED, F. (1994): Titanmobilität: Metasomatische, titanreiche Adern am Kontakt von Dolomitmarmoren zur Bergeller Intrusion, Ph. D. Thesis ETH Zürich, Switzerland, p. 204.

ROSSELL, H.J. (1980): Zirconolite – a fluorite-related superstructure. Nature 283, 282–283.

RYERSON, F.J. (1984): Phase equilibria of nuclear waste ceramics: the effect of oxygen fugacity. J. Am. Ceram. Soc. 67(2), 75–82.

SHANNON, R.D. (1976): Revised effective ionic radii and systematic studies of interatomic distances in halides and chalcogenides. Acta Cryst. A32, 751–767.

SHENG, Y.J., HUTCHEON, I.D. and WASSERBURG, G.J. (1991): Origin of plagioclase-olivine inclusions in carbonaceous chondrites. Geochim. Cosmochim. Acta 55, 581–599.

SINCLAIR, W. and EGGLETON, R.A. (1982): Structure refinement of zirkelite from Kaiserstuhl, West Germany. Am. Mineral. 67, 615–620.

SMITH, K.L., COLELLA, M., THOROGOOD, G.J., BLACKFORD, M.G., LUMPKIN, G.R., HART, K.P., PRINCE, K., LOI, E. and JOSTSONS, A. (1997): Dissolution of Synroc in deionised water at 150 °C. In: GRAY, W.J. and TRIAY, I.R. (eds): Scientific Basis for Nuclear Waste Management XX, 465, p. 349–354. Materials Research Society, Boston, USA.

SMITH, K.L. and LUMPKIN, G.R. (1993): Structural features of zirconolite, hollandite and perovskite, the major waste-bearing phases in Synroc. In: BOLAND, J.N. and FITZ GERALD, J.D. (eds): Defects and Processes in the Solid State: Geoscience Applications. Elsevier: The McLaren Volume, 401–422.

SONNENTHAL, E.L. (1992): Geochemistry of dendritic anorthosites and associated pegmatites in the Skaergaard Intrusion, East Greenland: Evidence for metasomatism by a chlorine-rich fluid. Journal of Volcanology and Geothermal Research 52, 209–230.

VANCE, E.R., BALL, C.J., DAY, R.A., SMITH, K.L., BLACKFORD, M.G., BEGG, B.D. and ANGEL, P.J. (1994): Actinide and rare earth incorporation into zirconolite. Journal of Alloys and Compounds 213/214, 406–409.

VANCE, E.R., BEGG, B.D., DAY, R.A. and BALL, C.J. (1995): Zirconolite-rich ceramics for actinide wastes.

Materials Research Society Symposium, 353, p. 767–774. Materials Research Society.

WHITE, T.J. (1984): The microstructure and microchemistry of synthetic zirconolite, zirkelite and related phases. Am. Mineral. 69, 1156–1172.

WHITE, T.J., SEGALL, R.L., HUTCHISON, J.L. and BARRY, J.C. (1984): Polytypic behaviour of zirconolite. Proceedings of the Royal Society, London A392, 343–358.

WILLIAMS, C.T. (1996): The occurrence of niobian zirconolite, pyrochlore and baddeleyite in the Kovdor carbonatite complex, Kola Peninsula, Russia. Mineral. Mag. 60, 639–646.

WILLIAMS, C.T. and GIERÉ, R. (1988): Metasomatic zonation of REE in zirconolite from a marble skarn at the Bergell contact aureole (Switzerland/Italy). Schweiz. Mineral. Petrogr. Mitt. 68, 133–140.

WILLIAMS, C.T. and GIERÉ, R. (1996): Zirconolite: a review of localities worldwide, and a compilation of its chemical compositions. Bulletin of the Natural History Museum, London (Geology) 52(1), 1–24.

ZAKRZEWSKI, M.A., LUSTENHOUWER, W.J., NUGTEREN, H.J. and WILLIAMS, C.T. (1992): Rare-earth minerals yttrian zirconolite and allanite-(Ce) and associated minerals from Koberg mine, Bergslagen, Sweden. Mineral. Mag. 56, 27–35.

Manuscript received January 7, 1998; revision accepted August 31, 1998.

Appendix

STATISTICAL DATA FOR ZIRCONOLITE FROM VARIOUS LOCALITIES

Tab. A1 **Kovdor** (n = 18; analyses C14–C34).

Descriptive statistics						**Correlation matrix**							
	Mean	σ_{n-1}	Min.	Max.	Range	Ca	ACT	REE	Me^{5+}	Ti	Mg	Fe_{tot}	Al
Ca	0.851	0.036	0.788	0.896	0.108	1.000							
ACT	0.055	0.024	0.022	0.100	0.078	–0.783	1.000						
REE	0.104	0.016	0.060	0.129	0.069	–0.338	–0.257	1.000					
Me^{5+}	0.613	0.081	0.447	0.744	0.297	–0.386	0.515	–0.122	1.000				
Ti	0.940	0.113	0.768	1.174	0.406	0.477	–0.561	0.031	–0.987	1.000			
Mg	0.054	0.018	0.026	0.082	0.056	–0.734	0.793	0.026	0.793	–0.853	1.000		
Fe_{tot}	0.417	0.020	0.375	0.446	0.071	–0.640	0.541	0.265	0.808	–0.861	0.887	1.000	
Al	0.000	0.000	0.000	0.000		•	•	•	•	•	•	•	•
Me^{2+}	0.484	0.039	0.407	0.537	0.130	–0.736	0.711	0.146	0.827	–0.884			•
Me^{3+}	0.417	0.020	0.375	0.446	0.071	–0.640	0.541	0.265	0.808	–0.861	0.887		
ΣM8	1.010	0.014	0.985	1.035	0.050								
ΣM7	0.992	0.016	0.958	1.018	0.060								
ΣM5,6	2.037	0.015	2.009	2.057	0.048								

Tab. A2 **Schryburt Lake** (n = 24; analyses C35–C58).

Descriptive statistics						**Correlation matrix**							
	Mean	σ_{n-1}	Min.	Max.	Range	Ca	ACT	REE	Me^{5+}	Ti	Mg	Fe_{tot}	Al
Ca	0.636	0.131	0.445	0.855	0.410								
ACT	0.032	0.024	0.002	0.121	0.119	0.395	1.000						
REE	0.324	0.137	0.139	0.567	0.428	–0.943	–0.590	1.000					
Me^{5+}	0.371	0.126	0.090	0.600	0.510	0.546	0.409	–0.613	1.000				
Ti	1.166	0.127	0.936	1.455	0.519	–0.381	–0.508	0.486	–0.947	1.000			
Mg	0.030	0.012	0.008	0.062	0.054	0.480	0.471	–0.559	0.352	–0.436	1.000		
Fe_{tot}	0.420	0.030	0.376	0.474	0.098	–0.402	–0.187	0.392	0.232	–0.294	–0.061	1.000	
Al	0.003	0.004	0.000	0.016	0.016	–0.006	0.470	–0.135	–0.380	0.255	0.414	–0.294	1.000
Me^{2+}	0.475	0.034	0.418	0.539	0.121	–0.353	0.048	0.245	0.346	–0.503			–0.082
Me^{3+}	0.423	0.029	0.383	0.477	0.094	–0.416	–0.123	0.385	0.183	–0.265	–0.001		
ΣM8	0.992	0.035	0.879	1.037	0.158								
ΣM7	1.021	0.038	0.972	1.108	0.136								
ΣM5,6	2.030	0.035	1.971	2.091	0.120								

Tab. A3 **Hegau** (n = 16; analyses C73–C88).

Descriptive statistics						**Correlation matrix**							
	Mean	σ_{n-1}	Min.	Max.	Range	Ca	ACT	REE	Me^{5+}	Ti	Mg	Fe_{tot}	Al
Ca	0.864	0.015	0.827	0.887	0.060								
ACT	0.041	0.007	0.031	0.058	0.027	–0.042	1.000						
REE	0.053	0.010	0.038	0.074	0.036	0.044	0.831	1.000					
Me^{5+}	0.345	0.102	0.225	0.557	0.332	0.266	0.828	0.900	1.000				
Ti	1.248	0.121	0.996	1.408	0.412	–0.235	–0.844	–0.905	–0.996	1.000			
Mg	0.034	0.007	0.027	0.051	0.024	–0.202	0.801	0.739	0.777	–0.804	1.000		
Fe_{tot}	0.363	0.035	0.314	0.432	0.118	0.151	0.824	0.855	0.966	–0.973	0.817	1.000	
Al	0.024	0.006	0.015	0.033	0.018	–0.433	–0.709	–0.794	–0.943	0.937	–0.605	–0.915	1.000
Me^{2+}	0.411	0.045	0.355	0.501	0.146	0.094	0.853	0.857	0.961	–0.971			–0.885
Me^{3+}	0.388	0.029	0.348	0.448	0.100	0.094	0.830	0.850	0.952	–0.962	0.842		
ΣM8	0.959	0.023	0.912	1.000	0.088								
ΣM7	1.077	0.039	1.001	1.127	0.126								
ΣM5,6	2.029	0.021	2.000	2.074	0.074								

Tab. A4 **Howard Creek** (n = 46; analyses C90–C135).

Descriptive statistics						**Correlation matrix**							
	Mean	σ_{n-1}	Min.	Max.	Range	Ca	ACT	REE	Me^{5+}	Ti	Mg	Fe_{tot}	Al
Ca	0.669	0.057	0.585	0.750	0.165								
ACT	0.213	0.076	0.108	0.307	0.199	–0.946	1.000						
REE	0.094	0.023	0.065	0.144	0.079	0.725	–0.899	1.000					
Me^{5+}	0.279	0.039	0.230	0.349	0.119	0.872	–0.899	0.759	1.000				
Ti	1.269	0.023	1.208	1.302	0.094	–0.481	0.542	–0.482	–0.831	1.000			
Mg	0.040	0.009	0.027	0.052	0.025	–0.919	0.980	–0.898	–0.855	0.482	1.000		
Fe_{tot}	0.449	0.019	0.387	0.473	0.086	–0.551	0.765	–0.866	–0.611	0.362	0.780	1.000	
Al	0.005	0.001	0.004	0.008	0.004	0.621	–0.599	0.481	0.526	–0.280	–0.573	–0.331	1.000
Me^{2+}	0.505	0.026	0.467	0.541	0.074	–0.869	0.957	–0.907	–0.795	0.407			–0.513
Me^{3+}	0.454	0.019	0.391	0.477	0.086	–0.531	0.748	–0.856	–0.595	0.354	0.765		
ΣM8	0.976	0.011	0.926	0.988	0.062								
ΣM7	1.007	0.019	0.976	1.057	0.081								
ΣM5,6	2.058	0.011	2.006	2.076	0.070								

Tab. A5a **Araxá, low-REE zirconolite** (n = 14; analyses C136–C139 and C152–C161).

Descriptive statistics						**Correlation matrix**							
	Mean	σ_{n-1}	Min.	Max.	Range	Ca	ACT	REE	Me^{5+}	Ti	Mg	Fe_{tot}	Al
Ca	0.860	0.013	0.833	0.878	0.045								
ACT	0.021	0.008	0.009	0.036	0.027	–0.802	1.000						
REE	0.097	0.009	0.077	0.109	0.032	–0.371	0.639	1.000					
Me^{5+}	0.138	0.049	0.057	0.187	0.130	–0.303	0.694	0.869	1.000				
Ti	1.568	0.073	1.478	1.695	0.217	0.436	–0.797	–0.821	–0.977	1.000			
Mg	0.014	0.004	0.007	0.021	0.014	–0.710	0.932	0.622	0.735	–0.839	1.000		
Fe_{tot}	0.270	0.033	0.208	0.312	0.104	–0.484	0.841	0.826	0.959	–0.988	0.848	1.000	
Al	0.006	0.002	0.000	0.008	0.008	0.059	0.432	0.604	0.800	–0.766	0.417	0.729	1.000
Me^{2+}	0.289	0.039	0.215	0.341	0.126	–0.527	0.866	0.815	0.946	–0.983			0.689
Me^{3+}	0.276	0.035	0.211	0.318	0.107	–0.457	0.828	0.825	0.965	–0.990	0.834		
ΣM8	0.978	0.013	0.955	0.994	0.039								
ΣM7	1.082	0.022	1.049	1.120	0.071								
ΣM5,6	2.004	0.017	1.976	2.026	0.050								

Tab. A5b **Araxá, high-REE zirconolite** (n = 12; analyses C140–C151).

Descriptive statistics						**Correlation matrix**							
	Mean	σ_{n-1}	Min.	Max.	Range	Ca	ACT	REE	Me^{5+}	Ti	Mg	Fe_{tot}	Al
Ca	0.676	0.045	0.595	0.756	0.161								
ACT	0.041	0.018	0.013	0.081	0.068	–0.264	1.000						
REE	0.289	0.043	0.214	0.376	0.162	–0.896	–0.152	1.000					
Me^{5+}	0.221	0.111	0.072	0.384	0.312	0.013	0.596	–0.369	1.000				
Ti	1.400	0.129	1.210	1.598	0.388	0.161	–0.661	0.219	–0.983	1.000			
Mg	0.028	0.012	0.010	0.053	0.043	–0.429	0.744	0.016	0.825	–0.894	1.000		
Fe_{tot}	0.389	0.026	0.338	0.422	0.084	–0.629	0.714	0.285	0.726	–0.835	0.867	1.000	
Al	0.000	0.000	0.000	0.000	0.000	•	•	•	•	•	•	•	
Me^{2+}	0.431	0.042	0.352	0.498	0.146	–0.573	0.746	0.195	0.790	–0.885			
Me^{3+}	0.389	0.026	0.338	0.422	0.084	–0.629	0.714	0.285	0.726	–0.835	0.867		
ΣM8	1.006	0.008	0.987	1.021	0.034								
ΣM7	1.009	0.027	0.975	1.049	0.075								
ΣM5,6	2.055	0.017	2.029	2.081	0.052								

Tab. A6a **Bergell** (n = 58; includes 15 EPMA analyses [M8–M22 in WILLIAMS and GIERÉ, 1996] and 43 AEM analyses [from LUMPKIN et al. 1994c]).

Descriptive statistics						**Correlation matrix**							
	Mean	σ_{n-1}	Min.	Max.	Range	Ca	ACT	REE	Me^{5+}	Ti	Mg	Fe_{tot}	Al
Ca	0.836	0.094	0.540	0.963	0.423								
ACT	0.035	0.026	0.003	0.120	0.117	–0.856	1.000						
REE	0.161	0.085	0.052	0.424	0.372	–0.949	0.754	1.000					
Me^{5+}	0.026	0.021	0.000	0.072	0.072	–0.818	0.711	0.806	1.000				
Ti	1.694	0.093	1.461	1.814	0.353	0.953	–0.825	–0.926	–0.872	1.000			
Mg	0.006	0.009	0.000	0.033	0.033	–0.267	0.155	0.193	0.038	–0.143	1.000		
Fe_{tot}	0.244	0.070	0.139	0.415	0.276	–0.961	0.886	0.933	0.851	–0.950	0.203	1.000	
Al	0.042	0.014	0.014	0.080	0.066	–0.499	0.414	0.484	0.449	–0.505	0.174	0.501	1.000
Me^{2+}	0.252	0.073	0.140	0.438	0.298	–0.962	0.876	0.926	0.821	–0.937			0.505
Me^{3+}	0.287	0.078	0.175	0.468	0.293	–0.953	0.870	0.926	0.845	–0.944	0.214		
ΣM8	1.032	0.027	0.954	1.121	0.167								
ΣM7	1.000	0.033	0.912	1.067	0.155								
ΣM5,6	2.030	0.032	1.958	2.118	0.160								

Tab. A6b **Bergell.** Linear regression data for ΣM7 vs x (n = 58; AEM and EPMA data; mdl = number of analyses with concentrations below minimum detectable limit).

x	**slope**	**intercept**	**r**	**mdl**	**x**	**slope**	**intercept**	**r**	**mdl**
ACT	–0.929 (±0.111)	1.033 (±0.005)	–0.745	0	LREE	0.199 (±0.250)	0.990 (±0.013)	0.105	0
Th	–1.309 (±0.341)	1.022 (±0.007)	–0.456	0	HREE	–1.028 (±0.121)	1.037 (±0.005)	–0.749	0
U	–1.199 (±0.152)	1.022 (±0.004)	–0.725	4	HREE+Y	–0.290 (±0.036)	1.032 (±0.005)	–0.732	0
REE	–0.267 (±0.037)	1.043 (±0.007)	–0.692	0					
La	1.440 (±0.527)	0.992 (±0.005)	0.343	23					
Ce	2.010 (±0.427)	0.957 (±0.010)	0.532	0					
Pr	–3.068 (±2.312)	1.004 (±0.005)	–0.175	36					
Nd	–2.106 (±0.701)	1.034 (±0.012)	–0.373	0					
Sm	–5.498 (±0.737)	1.024 (±0.004)	–0.706	18					
Gd	–4.133 (±0.471)	1.023 (±0.004)	–0.761	20					
Dy	–2.397 (±0.342)	1.033 (±0.006)	–0.683	0					
Er	–4.022 (±0.459)	1.031 (±0.005)	–0.760	8					
Yb	–3.115 (±0.810)	1.027 (±0.008)	–0.457	7					
Y	–0.393 (±0.051)	1.030 (±0.005)	–0.715	0					

Tab. A7a **Adamello, low-REE zirconolite** (n = 74; includes 25 EPMA analyses [from WILLIAMS and GIERÉ, 1996] and 49 AEM analyses, unpublished).

Descriptive statistics						**Correlation matrix**							
	Mean	σ_{n-1}	Min.	Max.	Range	Ca	ACT	REE	Me^{5+}	Ti	Mg	Fe_{tot}	Al
Ca	0.776	0.080	0.603	1.042	0.439								
ACT	0.198	0.099	0.019	0.475	0.456	–0.921	1.000						
REE	0.077	0.022	0.018	0.118	0.100	0.106	–0.369	1.000					
Me^{5+}	0.029	0.015	0.011	0.075	0.064	–0.436	0.585	–0.458	1.000				
Ti	1.633	0.108	1.410	1.960	0.550	0.947	–0.905	0.079	–0.447	1.000			
Mg	0.070	0.071	0.006	0.269	0.263	–0.593	0.755	–0.590	0.850	–0.594	1.000		
Fe_{tot}	0.174	0.074	0.035	0.325	0.290	–0.684	0.569	0.297	–0.088	–0.725	–0.005	1.000	
Al	0.091	0.023	0.028	0.129	0.101	0.074	–0.298	0.505	–0.667	0.080	–0.613	0.296	1.000
Me^{2+}	0.252	0.106	0.052	0.473	0.421	–0.910	0.932	–0.179	0.508	–0.940			–0.192
Me^{3+}	0.265	0.083	0.090	0.422	0.332	–0.586	0.423	0.400	–0.259	–0.620	–0.171		
ΣM8	1.050	0.030	1.011	1.174	0.163								
ΣM7	0.980	0.039	0.871	1.055	0.184								
ΣM5,6	2.012	0.034	1.949	2.122	0.173								

Tab. A7b **Adamello, high-REE zirconolite** (n = 25; includes 14 EPMA analyses [from WILLIAMS and GIERÉ, 1996] and 11 unpublished AEM analyses).

Descriptive statistics						**Correlation matrix**							
	Mean	σ_{n-1}	Min.	Max.	Range	Ca	ACT	REE	Me^{5+}	Ti	Mg	Fe_{tot}	Al
Ca	0.691	0.095	0.519	0.853	0.334								
ACT	0.146	0.051	0.096	0.341	0.245	0.166	1.000						
REE	0.254	0.103	0.122	0.407	0.285	–0.837	–0.492	1.000					
Me^{5+}	0.070	0.030	0.021	0.125	0.104	–0.657	–0.304	0.815	1.000				
Ti	1.558	0.088	1.406	1.685	0.279	0.624	0.151	–0.748	–0.805	1.000			
Mg	0.088	0.041	0.025	0.204	0.179	0.153	0.557	–0.278	0.015	0.217	1.000		
Fe_{tot}	0.264	0.136	0.106	0.460	0.354	–0.639	–0.348	0.762	0.615	–0.862	–0.604	1.000	
Al	0.057	0.021	0.022	0.108	0.086	0.491	0.158	–0.635	–0.632	0.707	0.248	–0.742	1.000
Me^{2+}	0.362	0.119	0.180	0.532	0.352	–0.698	–0.208	0.792	0.728	–0.940			–0.777
Me^{3+}	0.322	0.121	0.155	0.505	0.350	–0.632	–0.363	0.744	0.580	–0.844	–0.635		
ΣM8	1.091	0.048	1.013	1.215	0.202								
ΣM7	0.937	0.042	0.829	0.994	0.165								
ΣM5,6	2.053	0.050	1.954	2.132	0.178								

Tab. A8 **Koberg** (n = 28; analyses M67–M94).

Descriptive statistics						**Correlation matrix**							
	Mean	σ_{n-1}	Min.	Max.	Range	Ca	ACT	REE	Me^{5+}	Ti	Mg	Fe_{tot}	Al
Ca	0.577	0.038	0.527	0.666	0.139								
ACT	0.046	0.018	0.017	0.074	0.056	–0.102	1.000						
REE	0.408	0.025	0.351	0.452	0.102	–0.495	–0.046	1.000					
Me^{5+}	0.091	0.020	0.057	0.133	0.077	–0.268	–0.340	0.720	1.000				
Ti	1.445	0.027	1.403	1.508	0.106	0.601	–0.133	–0.443	–0.495	1.000			
Mg	0.043	0.027	0.018	0.136	0.118	–0.305	0.061	–0.340	–0.276	–0.444	1.000		
Fe_{tot}	0.364	0.055	0.184	0.423	0.239	–0.713	–0.300	0.150	0.129	–0.230	0.115	1.000	
Al	0.024	0.011	0.008	0.060	0.052	–0.249	0.023	–0.549	–0.483	–0.238	0.914	0.233	1.000
Me^{2+}	0.458	0.048	0.325	0.574	0.249	–0.767	–0.160	0.049	0.053	–0.534			0.624
Me^{3+}	0.388	0.059	0.193	0.463	0.271	–0.717	–0.278	0.038	0.031	–0.261	0.280		
ΣM8	1.030	0.036	0.958	1.134	0.175								
ΣM7	1.016	0.016	0.989	1.052	0.063								
ΣM5,6	2.050	0.051	1.928	2.196	0.268								

Tab. A9 **Lunar basalts** (n = 9; analyses L1–L4 and L9–L13).

Descriptive statistics						**Correlation matrix**							
	Mean	σ_{n-1}	Min.	Max.	Range	Ca	ACT	REE	Me^{5+}	Ti	Mg	Fe_{tot}	Al
Ca	0.354	0.184	0.194	0.705	0.511								
ACT	0.007	0.007	0.000	0.021	0.021	0.641	1.000						
REE	0.511	0.294	0.130	0.910	0.780	–0.866	–0.818	1.000					
Me^{5+}	0.047	0.051	0.000	0.127	0.127	–0.443	–0.116	0.077	1.000				
Ti	1.400	0.092	1.308	1.577	0.268	0.262	0.231	–0.303	–0.086	1.000			
Mg	0.025	0.029	0.000	0.065	0.065	0.700	0.714	–0.773	–0.448	0.492	1.000		
Fe_{tot}	0.419	0.128	0.221	0.566	0.345	–0.932	–0.798	0.884	0.506	–0.184	–0.811	1.000	
Al	0.060	0.038	0.000	0.116	0.116	0.808	0.603	–0.865	–0.185	0.080	0.753	–0.801	1.000
Me^{2+}	0.446	0.106	0.256	0.573	0.317	–0.933	–0.762	0.851	0.501	–0.081			–0.762
Me^{3+}	0.491	0.088	0.366	0.627	0.261	–0.863	–0.774	0.768	0.589	–0.187	–0.708		
ΣM8	0.872	0.158	0.704	1.157	0.453								
ΣM7	1.155	0.130	1.023	1.361	0.338								
ΣM5,6	2.006	0.127	1.838	2.166	0.328								